AD-A064 688 AIR FORCE INST OF TECH WRIGHT-PATTERSON AFB OHIO SCH--ETC F/G 17/8
PARAMETRIC ANALYSIS OF STEREOMETRIC TRACKER FOR USE IN TACTICAL--ETC(U)
OCT 78 K F SCHROEDER

UNCLASSIFIED AFIT/GEP/PH/78D-11 NL

1 OF 2
AD
A064686

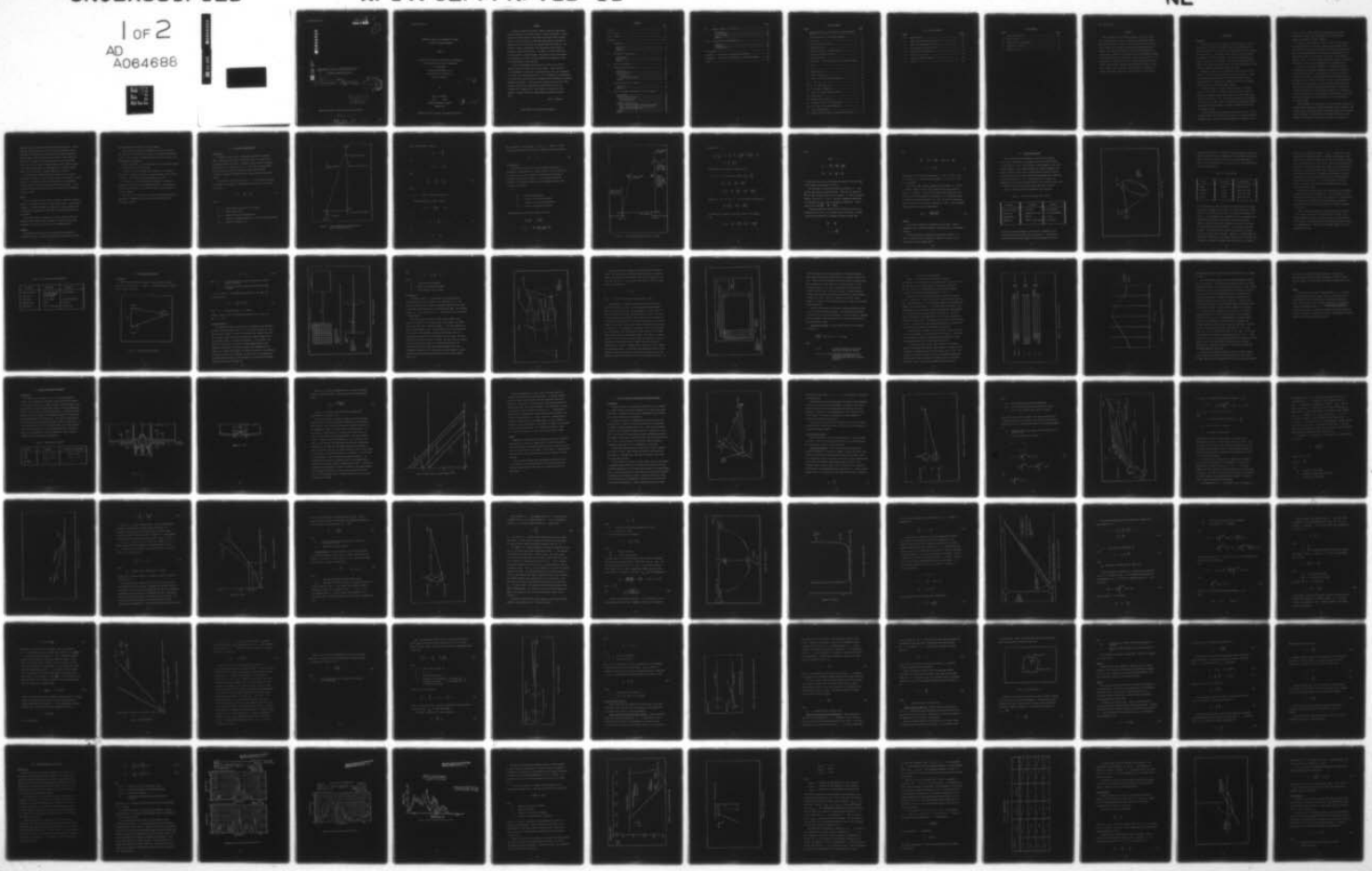

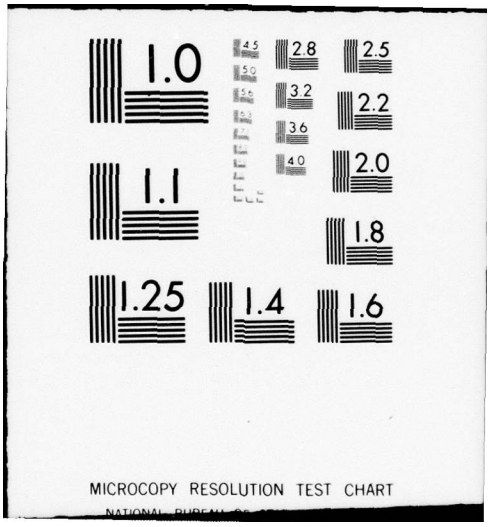
1.0
1.1
1.25
1.4
1.6
1.8
2.0
2.2
2.5
2.8
3.2
3.6
4.0
4.5
5.0
MICROCOPY RESOLUTION TEST CHART

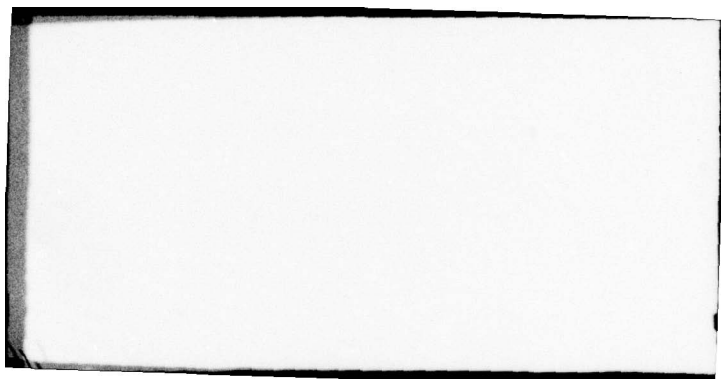

AFIT/GEP/PH/78D-11

LEVEL II

(1)

AD A064688

DDC FILE COPY

(6) PARAMETRIC ANALYSIS OF STEREOMETRIC TRACKER FOR USE IN TACTICAL AIRCRAFT.

(9) Master's THESIS,

(14) AFIT/GEP/PH/78D-11

(10) Kurt F. Schroeder
Capt USAF

(11) Oct 78

(12) 114p.

Approved for public release; distribution unlimited.

012 225

79 01 30 140

bpg

AFIT/GEP/PH/78D-11

PARAMETRIC ANALYSIS OF STEREOMETRIC TRACKER FOR USE IN TACTICAL AIRCRAFT

THESIS

Presented to the Faculty of the School of Engineering

of the Air Force Institute of Technology

Air University

in Partial Fulfillment of the

Requirements for the Degree of

Master of Science

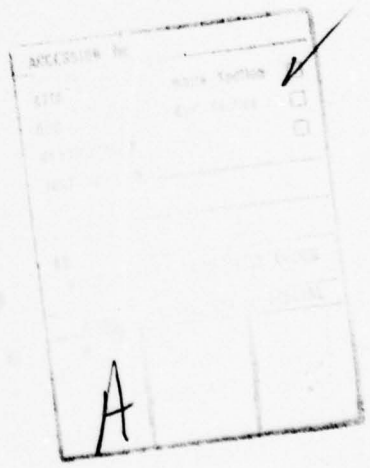

by

Kurt F. Schroeder

Capt USAF

Graduate Engineering Physics

October 1978

Preface

A means of passively tracking a target in range has been sought since the beginning of tracking systems. Recent developments in solid state electro-optic detectors have made very accurate angle tracking possible. At the same time, solid state technology has also made it possible to process video data very rapidly using small devices. The result is a small, light-weight, high resolution sensor capable of following a target at high rates. The impact of aircraft vibrations on these sensors is not well known. The purpose of this investigation is to determine the effects that the vibration environment will have on the functioning of these devices.

I wish to acknowledge the help of Mr. W. Frost for his help in obtaining flight test data vital to this thesis. Capt Paul Whaley of the Department of Aeronautics and Astronautics, AFIT, gave generously of his time in interpreting the data. Dr. D. Shankland of the Department of Physics, AFIT, was very helpful throughout this investigation, providing guidance and insight. I wish to thank Dr. Harold Rose of the Air Force Avionics Laboratory for proposing this thesis topic and for his valuable aid in completing it. And finally, my thanks to my wife, Beverly, for moral support and understanding throughout my stay at AFIT.

Kurt F. Schroeder

(This thesis was typed by Sharon Gabriel)

Contents

List of Figures

List of Figures (Cont'd)

List of Tables

Abstract

The stereometric range finding technique is used as the basis of an airborne passive tracker. An analysis of the method reveals that angular accuracy is the most critical element in this technique. Range accuracy can be improved by increasing baseline separation. However, the vibration environment of the aircraft becomes worse as the baseline is increased. The results of this investigation indicate that these vibrations can counter most of the gain in resolution. The investigation is hindered by a lack of vibrational data, especially angular vibration data. However, the investigation establishes what data is needed, and how such data can be applied, once obtained, to estimate performance potential of the stereometric ranging method.

I. Introduction

Background

Fighter aircraft perform a number of different missions. These missions can be divided into air-to-air and air-to-ground missions. In air-to-air missions, the target is an airborne object such as another aircraft or missile. Intercepts, escort, and close-in aerial combat are examples of air-to-air missions. In air-to-ground missions, the fighter's target is on the ground. Such targets include enemy tanks, bridges, air fields and logistics areas. Air-to-ground missions include close-air support, interdiction and airfield attack.

Whether the target is on the ground or in the air, the aircrew's mission is to find it and put ordnance on it when required. In order to successfully complete the mission without unnecessary risks to aircraft and crews, sophisticated tracking, fire control and weapons release systems are installed on USAF fighters.

Tracking systems are used to follow the motion of the target relative to the fighter. Information from the tracking systems is processed to determine target range, range rate, line-of-sight (LOS) angle and angular rate. Fire control systems present this information to the crew in a suitable format. Weapon release systems use tracking information along with fighter state data to compute weapon release or to launch signals.

Tracking systems can be classified as passive or active. Active tracking systems are those which direct energy at the target and track reflected energy. Radars and laser designators are examples of such

systems. Passive tracking systems are those which track energy emitted by the target. Heat seeking devices and electro-optic trackers are examples of passive trackers.

At present, fighters must use active trackers to measure target range and range rate in real time. However, active trackers alert the target to the presence of the fighter. This gives the enemy forces time to take evasive maneuvers, use electronic countermeasures, fire homing missiles back at the fighter or take cover. The element of surprise is lost. Not only does this decrease the chances of destroying the target, it also increases the hazards to the attacking force.

For example, according to Reference 1, the McDonnell Douglas F-4 Phantom has only limited capability to attack a MIG 25 Foxbat at 80,000 feet and Mach 2.0+. This would surely be negated if the F-4 were to use its radar, an active system, and alert the Foxbat that it was under attack. But the F-4 must use its radar to detect and track the Foxbat. For this example, a passive tracking system which has a range tracking capability would increase the success of the mission. It would be possible to use the tracking information to intercept the target at optimum missile launch parameters before turning on the radar for missile guidance. The first indication of the attack would be the missile launch.

Another example of the advantage of a passive tracker is the case of a single fighter attacking a ground target deep in enemy territory. For mission success and fighter survival, such missions rely on one surprise pass at the target. This means that the fighter should not emit any energy as it navigates to the target. Accuracy of the bomb run is

important since the aircrew can afford to make only one pass. On the bomb run, the crew would like to go in as fast as possible, fly an unpredictable flight path and keep look-out for enemy surface-to-air missiles (SAM). This means that the actual bomb release would best be done by an automatic weapons release system. But such systems often rely on target range information from an active tracking system. Such a system is vulnerable to countermeasures. A passive tracking system is less vulnerable and almost impossible to detect.

Present passive tracking systems in fighters are LOS trackers only. What is needed is a passive system which is also capable of range tracking. An extension of the LOS tracker would be a stereometric system composed of two such trackers separated by a baseline. It will be shown later that this system requires very accurate LOS performance from the trackers.

Purpose

It is the purpose of this report to perform a parametric trade-off analysis of a passive stereometric range finding system. Sensor angular resolution, aircraft vibration and flexures, and sensor baseline will be analyzed to determine their effect on the range finding accuracy of this system.

This analysis will be applied to a specific fighter aircraft to determine sensor specifications required to achieve practical range accuracies for various air-to-air and air-to-ground missions.

Approach

This analysis will start with a discussion of the theory of stereometric ranging. An error analysis will be performed to disclose

the most important parameters for range accuracy.

Some criteria for tracker performance are assessed, starting with contract specifications for research on an advanced stereometric tracker. The criteria are expanded to meet the air-to-air and air-to-ground mission requirements.

Angular resolution of a focal plane sensor is investigated as well as the means used to track the target.

In order to increase maximum range capability of the tracker, the effect of placing two trackers at remote locations on the aircraft is studied. Some typical aircraft dimensions are given.

The effect of aircraft vibration and flexures are presented. Analytical equations are formed whenever possible. The expressions derived from this analysis are used to evaluate sensor placement on a typical fighter.

The last section contains the conclusions from the analysis and appropriate recommendations are made for the development of the stereometric tracker.

II. Stereometric Range Method

Introduction

Stereometric range theory is most easily presented in geometric terms. One measures the line of sight (LOS) angle to an object from two positions along a baseline. In Figure 1, the LOS angle is measured with the help of a reference line, RL . This line is perpendicular to the base and in the plane formed by the baseline and target. Parallax is measured by aligning the tip of the reference line and the target.

The difference in the LOS angles is α . In the special case when the target LOS is parallel to the reference line (Fig. 1), it is easy to see that

$$\tan \alpha = \frac{B}{R_2} = \frac{P}{RL} \qquad (1)$$

where

α = angle formed by both LOS's at the target

B = baseline separation

R_2 = range to the target from position 2

P = parallax in sighting angle due to a shift in viewing position

RL = length of reference line

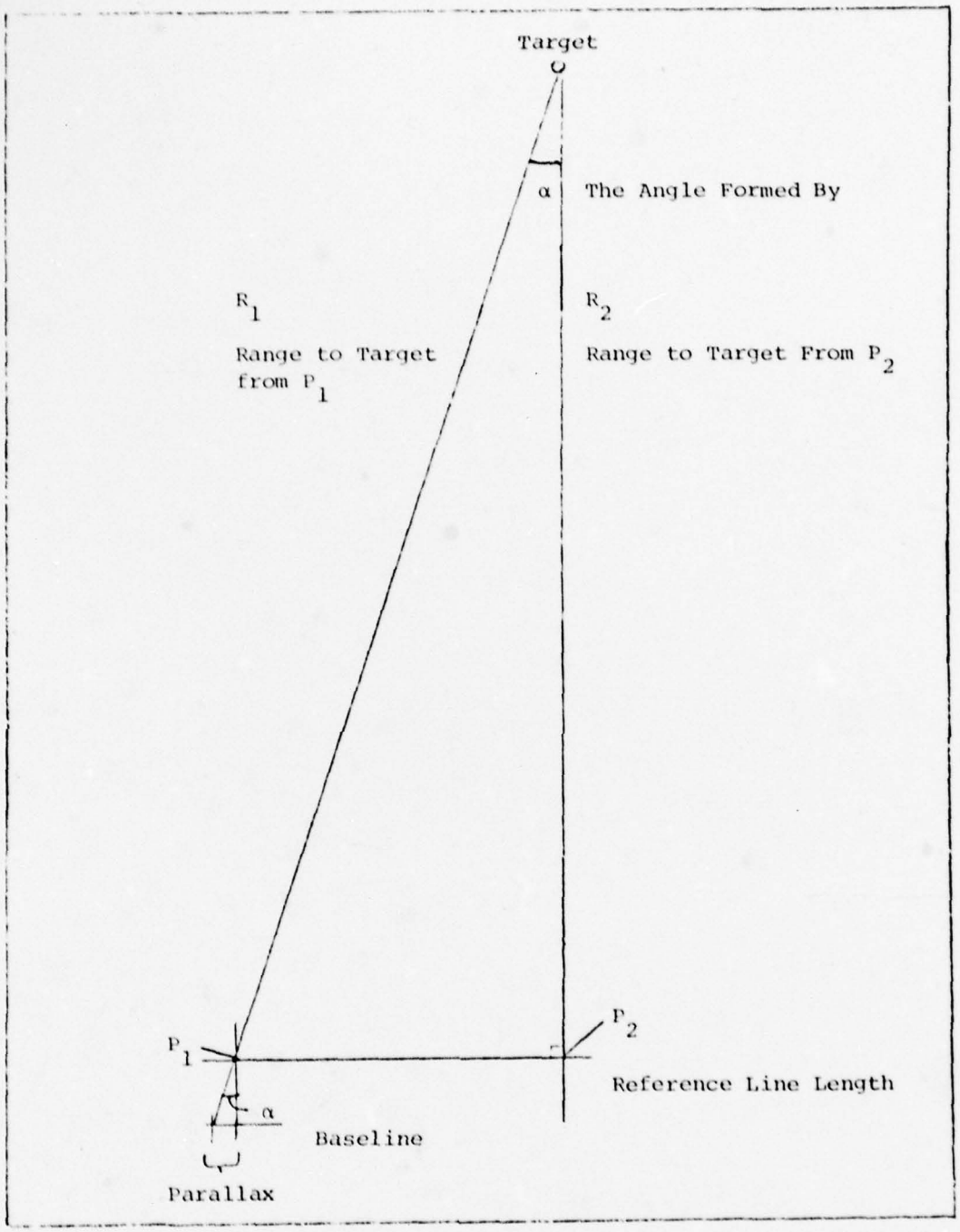

Figure 1. Range Measurement by Triangulation - The Stereometric Method

Also, with the help of Figure 1

$$\sin \alpha \approx \frac{B}{R_1}$$

If

$$\sin \alpha \approx \tan \alpha$$

then

$$\frac{B}{R_1} \approx \frac{B}{R_2} = \frac{P}{RL} \qquad (2)$$

where

R_1 = range to target from position 1.

The approximation is valid as long as

$$\tan \alpha = \frac{\sin \alpha}{\cos \alpha} \approx \sin \alpha$$

or

$$\cos \alpha = \frac{R_2}{R_1} \approx 1 \qquad (3)$$

or

$$R_1 \approx R_2$$

For the purpose of this analysis, $R_1 = R_2 = R$, where R is the range to the target from either sensor. Equation 2 will be written as

$$\frac{B}{R} = \frac{P}{F} = \alpha \tag{4}$$

Error Analysis

This paper will analyze the range tracking capability of a stereometric system mounted on a fighter aircraft. Such a system will be composed of two sensors capable of measuring image shift due to baseline separation (see Figure 2). It is important to know the parameters in Equation (4) which will limit maximum range and range accuracy of the system.

Let

ΔR = range accuracy desired

ΔB = accuracy of baseline measurement

ΔF = accuracy of focal length measurement

ΔP = accuracy of parallax measurement

Substituting these values into Equation (4) gives

$$\frac{R + \Delta R}{B + \Delta B} = \frac{F + \Delta F}{P + \Delta P}$$

$$R + \Delta R = \frac{FB + \Delta FB + F\Delta B + \Delta F\Delta B}{(P + \Delta P)}$$

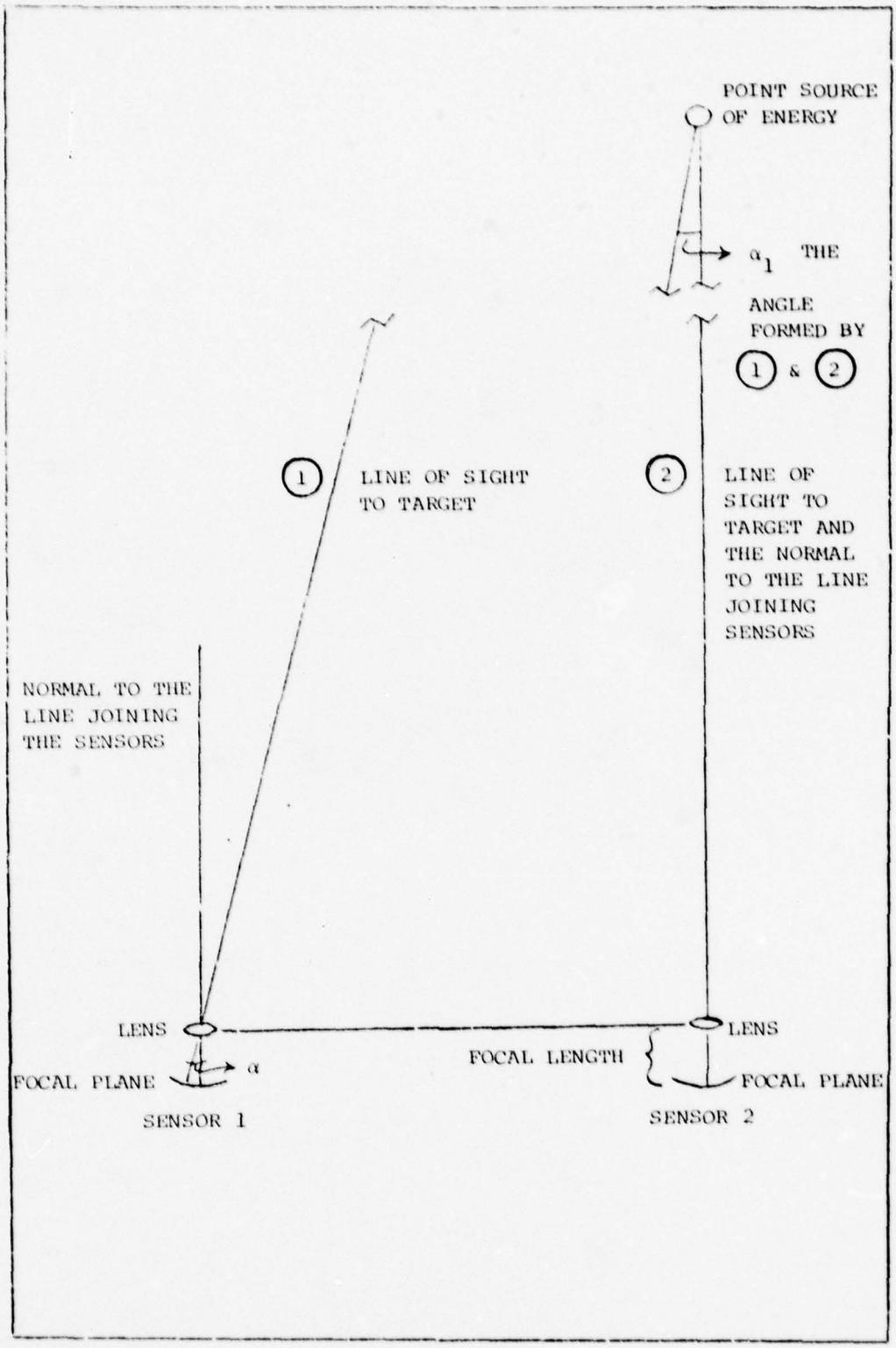

FIGURE 2. Range Measurement by Stereometric Method

Assuming $\Delta P << P$,

$$\frac{1}{P\left(1 + \frac{\Delta P}{P}\right)} = \frac{1}{P}\left[1 - \frac{\Delta P}{P} + \left(\frac{\Delta P}{P}\right)^2 - \left(\frac{\Delta P}{P}\right)^3 + \ldots\right]$$

$$\approx \frac{1}{P}\left[1 - \frac{\Delta P}{P}\right]$$

Substitution into the previous equation gives

$$R + \Delta R = [FB + \Delta FB + F\Delta B + \Delta F\Delta B]\ \frac{1}{P}\left(1 - \frac{\Delta P}{P}\right)$$

$$= \frac{FB}{P} + \frac{\Delta FB}{P} + \frac{F\Delta B}{P} + \frac{\Delta F\Delta B}{P}$$

$$- \Delta P\ \frac{FB}{P^2} - \frac{\Delta P}{P}\left[\frac{\Delta FB}{P} + \frac{F\Delta B}{P} + \frac{\Delta F\Delta B}{P}\right]$$

Assuming $\Delta F << F$ and $\Delta B << B$, the last term in this equation

$$- \frac{\Delta P}{P}\left[\frac{\Delta FB}{P} + \frac{F\Delta B}{P} + \frac{\Delta F\Delta B}{P}\right]$$

is insignificant compared to the other terms in the equation.

Thus,

$$R + \Delta R = \frac{FB}{P} + \frac{\Delta FB}{P} + \frac{F\Delta B}{P} + \frac{(-)FB\Delta P}{P^2}$$

Since

$$\frac{FB}{P} = R$$

$$\Delta R = \frac{\Delta FB}{P} + \frac{F\Delta B}{P} + \frac{FB\Delta P}{P^2}$$

$$\frac{\Delta R}{R} = \frac{\Delta F}{F} + \frac{\Delta B}{B} + \frac{\Delta P}{P}$$

In words then, the sum of the parameters expressed as ratios is equal to the range error expressed as a ratio.

This analysis is concerned with angular resolution, α , and baseline separation on ranging accuracy. Therefore, the effects of $\frac{\Delta B}{B}$ and $\frac{\Delta F}{F}$ on range accuracy will be ignored. As a word of caution, however, the error in F and B cannot be ignored when specifying the tolerances for sensor optics and baseline separation. It will always be at least $\left[\frac{\Delta F}{F} + \frac{\Delta B}{B} \leq \frac{\Delta R}{R}\right]$.

It appears that range accuracy is not affected by the error in parallax any more than it is affected by error in baseline. However, if baseline and parallax are expressed in terms of range, then

$$\frac{\Delta R}{R} = \frac{\Delta B}{B}$$

$$R = R\frac{\Delta B}{B} \qquad (5)$$

and

$$\frac{\Delta R}{R} = \frac{\Delta P}{P} = R\,\frac{\Delta P}{FB} \quad , \quad \text{since} \quad \frac{1}{P} = \frac{R}{FB}$$

$$\Delta R = R^2\,\frac{P}{FB} \tag{6}$$

The quantity ΔR increases linearly with R, once ΔB and B are set. However, ΔR increases with the square of R if ΔP, F and B are constant.

If the ratio $\frac{\Delta R}{R}$ is made a constant for all ranges, ΔB is also a constant. However, keeping $\frac{\Delta R}{R}$ constant for all ranges does not make ΔP a constant. It still varies linearly with range and it will be the most critical parameter at long ranges. If a particular system is capable of measuring parallax to ΔP and the system is required to measure range to a given accuracy, expressed as $\Delta R/R$, then the maximum range of the system is set by Equation (6)

$$R_{max} = \left(\frac{\Delta R}{R}\right)\left(\frac{FB}{\Delta P}\right) \quad . \tag{6a}$$

Summary

This section examined the stereometric range theory. Several assumptions were necessary to maintain a simplified form of the ranging equation.

An error analysis was performed on the ranging equation. In order to extend the range capability of system, it appears that ΔP will prove to be the limiting term.

III. Tracker Requirements

This section will list performance criteria for the tracker. These criteria are based on a statement of work for Contract F33615-78-C-1562 (Ref. 1). The criteria stated in that document are for close-in aerial gunfire. This environment makes the greatest demand on the tracker in terms of angle rates. Maximum range of current air-to-air intercept missiles are used to estimate desired maximum range capability of the tracker (Refs. 2, 3, 4). The desired field of regard is a combination of the field of regard required in the contract and the field of regard for the Pave Tack system quote in Reference 5, page 57.

Table I shows the parameter requirements from Reference 1.

Table I. List of CAI Criteria (Ref. 1:A6-7)

Parameter	Magnitude	Accuracy
Field of Regard	120° Cone	$\leq$ 1 milliradian
Angle Rate	Maximum of 60°/sec	$\leq$ 4 milliradians/sec
Maximum Range	4000 ft	$\leq \pm$ 50 ft
Range Rate	+500 to -1600 ft/sec	$\leq \pm$ 50 ft/sec

The field of regard parameter of a 120° cone is referenced to the aircraft fuselage longitudinal axis (see Figure 3). The article on Pave Tack states that that system has a full hemispherical field of

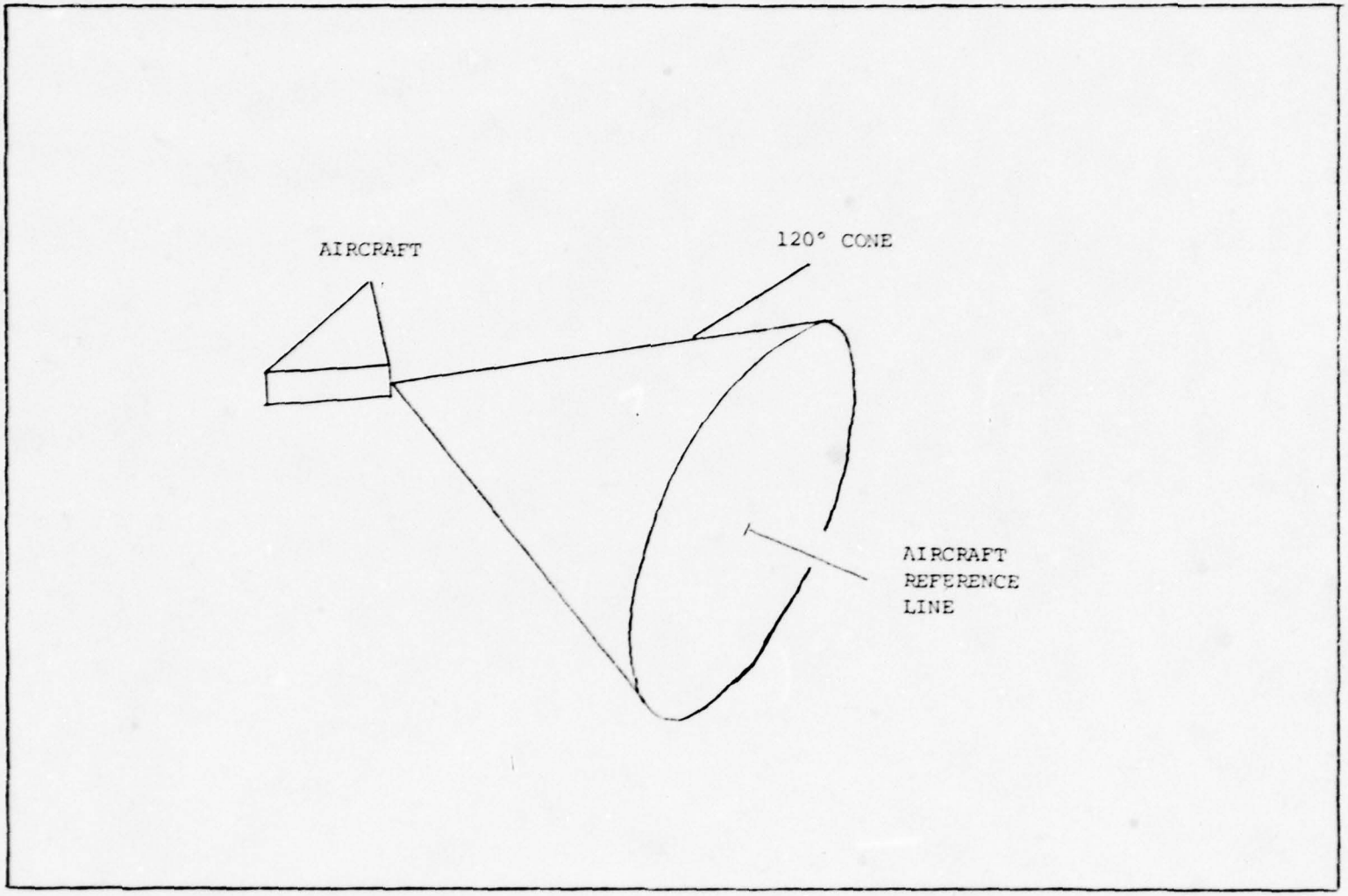

FIGURE 3. 120° Cone

regard below the aircraft. The field of regard requirement, then, will expand to include the lower hemisphere also. The maximum range requirement has little use outside of an air-to-air gun tracking mission. Table II gives maximum ranges of some current air-to-air guided missiles from unclassified sources.

Table II. Missile Ranges

Name	Designation	Maximum Range
Falcon	AIM-4A	5+NM (Ref 4:82)
Sidewinder	AIM-9C	10NM (Ref 4:114)
Sparrow	AIM-7F	24+NM (Ref 3:82)
Phoenix	AIM-54	89NM (Ref 2:56)

To be compatible with these missiles and future missiles, the tracker should have a maximum range of 89 NM. It is often desirable to launch a missile at a range which will give it the greatest probability for a kill. If this optimum range is assumed to be half the maximum range, then tracking beyond that range might be considered unnecessary. However, a fighter often wishes to improve its position with respect to the target prior to missile launch. To do so requires time and distance. If the fighter and its target are closing at 1000 knots, they close 16-2/3 miles every minute. Therefore, if optimum range for the AIM-54 is 89NM/2 and if the fighter requires about two minutes prior to launch for maneuvering, maximum range capability of the tracking

system is 2(16 2/3)NM + 44 1/2NM = 77 NM . The AIM-54 is a long range missile. Maximum tracking for the other missiles varies from 45 NM to 35 NM. For the purposes of this thesis, the maximum tracking range of the system will be set at 89 NM. This range could easily be twice what is actually required if the fighter is not compatible with the AIM-54, or if missile launch range is restricted to even shorter ranges due to other factors. Maximum tracking capability has been assessed using air-to-air missiles because air-to-ground ordnance typically has shorter range. If the range accuracy of 50 ft at 4000 ft, as stated in the contract, is extended to 89 NM, range accuracy would be 1.1 NM.

The -1600 ft/sec range rate is not sufficient for two supersonic fighters closing head-on (Reference 6). In the reference cited, two fighters were closing at Mach 4.0. This converts to a closing rate of up to -4350 ft/sec, depending on precise atmospheric conditions. Maintaining the range rate accuracy ratio, the accuracy requirement is 136 ft/sec.

Both the range and range rate accuracy requirements in Table I were to predict the path of a bullet fired from a fighter. The predicted bullet trajectory is used to generate an aiming reference for the pilot. This requirment may be more restrictive than required for a guided missile. Table III lists revised parameters for the stereometric tracker.

Table III. Revised Tracker Requirements

Parameter	Magnitude	Accuracy
Field of Regard	120° Cone forward plus Hemisphere below aircraft	≤ 1 milliradian
Angle Rate		
Angle Rate	60°/sec (Max)	≤ 4 milliradians/sec
Maximum Range	89NM	≤ ±1.1 NM
Range Rate	500 to -4350 ft/sec	≤ ±136 ft/sec

IV. System Angular Resolution

Introduction

Maximum range capability and range accuracy depend on how well the angle α can be measured. Angle α is the LOS difference between the two sensors (Figure 4).

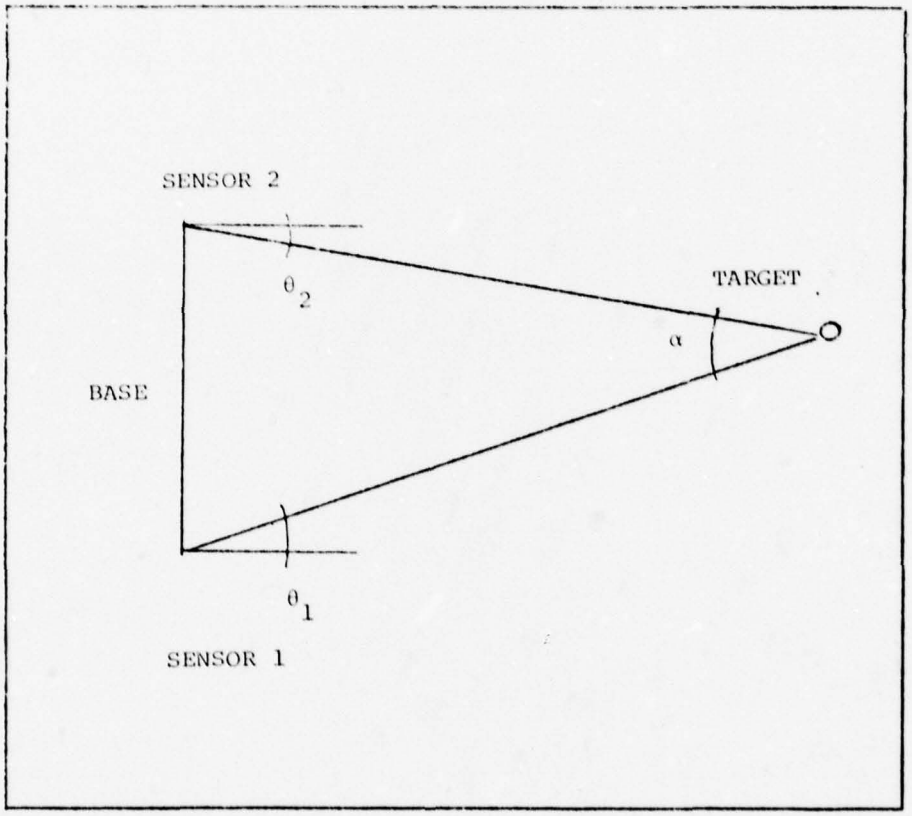

Figure 4. Top View of Stereo System

$$\alpha = \theta_1 - \theta_2 \tag{6.1}$$

where θ_1 = LOS angle measured by sensor 1 relative to a vector normal to the base

θ_2 = LOS angle measured by sensor 2 relative to the same reference

If θ_1 and θ_2 are measured to an accuracy of $\Delta\theta_1$ and $\Delta\theta_2$, respectively, then

$$\Delta\alpha = \sqrt{\Delta\theta_1^2 + \Delta\theta_2^2} \tag{7}$$

where $\Delta\alpha$ = accuracy to which α is known.

Ideally, sensors 1 and 2 are manufactured such that $\Delta\theta_1 = \Delta\theta_2 = \Delta\theta$ and $\Delta\alpha = \sqrt{2}\,\Delta\theta$.

Sensor Resolution

The angular resolution of the sensor is determined by the detector's smallest resolution element (Ref. 7:1). For a sensor composed of a lens which focuses an image on an array of photosensitive elements, the limit of resolution is the area of one photosensitive element divided by the focal length squared. The units are steradians. If the image of the target is smaller than one resolution element, the response of that element is the same as if the entire element were illuminated by the image. For a stereo range finder, the angular resolution in the direction parallel to the base is of interest. In this case, it is meaningful to describe angular resolution as the dimension of a photosensitive element parallel to the base (see Figure 5).

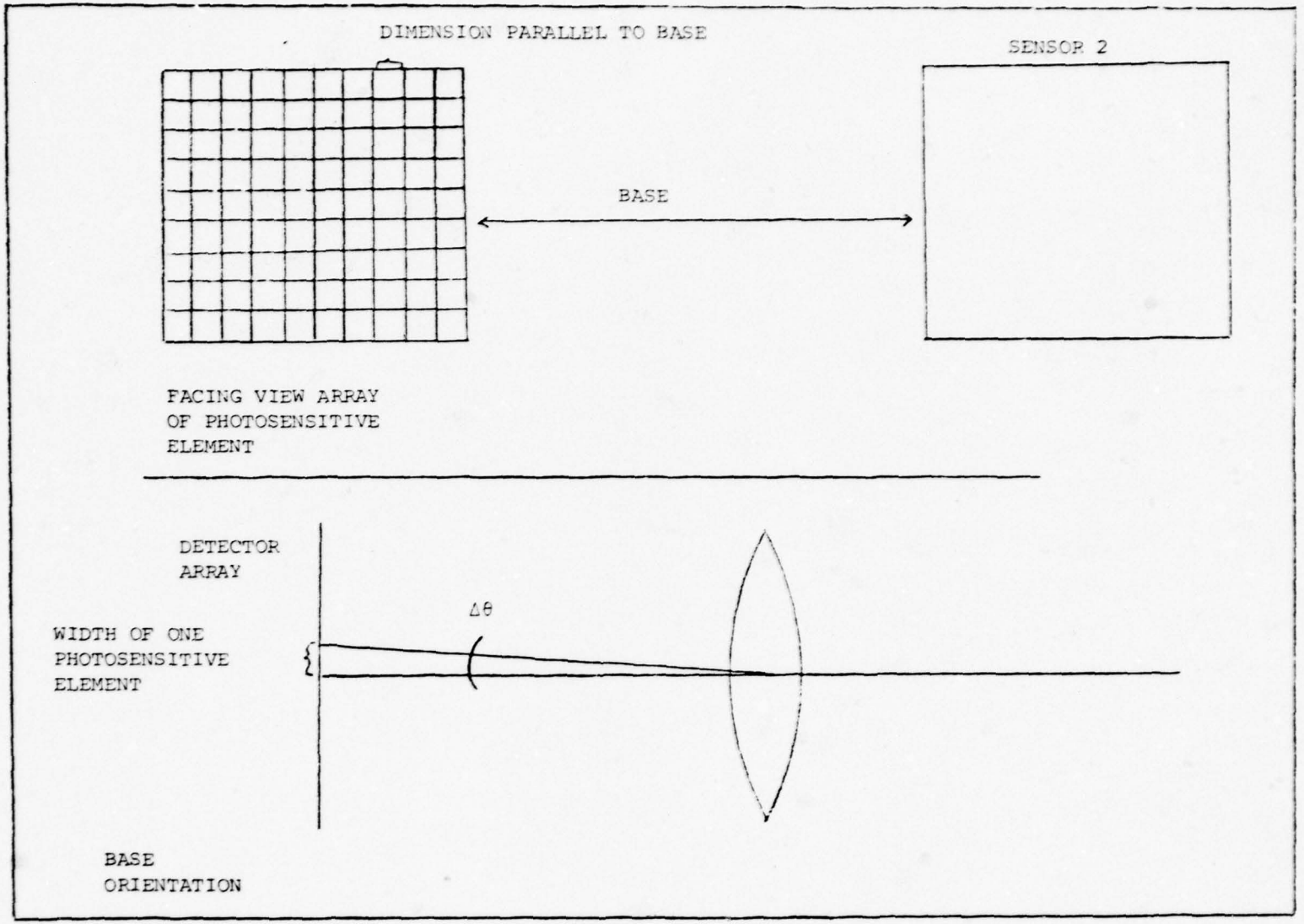

FIGURE 5. Angular Resolution

Then

$$\Delta\theta = \sin^{-1}\frac{p}{F} \qquad \frac{p}{F}$$

where

$\Delta\theta$ = is measured in milliradians

p = width of photosensitive element

F = focal length of optical system

CAI Proposal

The manner in which α is measured can be improved using a proposal by CAI, Division of Bourns, Inc. (Reference 8). In this proposal, the image in one sensor is compared directly with the image in the other sensor by means of a correlation algorithm. The resulting accuracy in α is a fraction of $\Delta\theta$. The following is a description of that proposal.

The passive tracker consists of three sensor systems in one housing (see Figure 6). The stereo base is four inches. The middle lens focuses the target on detector number 2. All three detectors are charge coupled devices (CCD). These detectors are in the focal plane of the lenses. The detectors record the target image over one integration period (Ref. 9:58) and produce a video signal. The video signal from the center detector is stored. The next signal is compared to the stored signal by means of a correlation algorithm. The misregistration in successive image signals computed using this correlation algorithm is used to produce correction signals to servo-mechanism controlling the pointing direction of the entire housing (Ref 8:2.6).

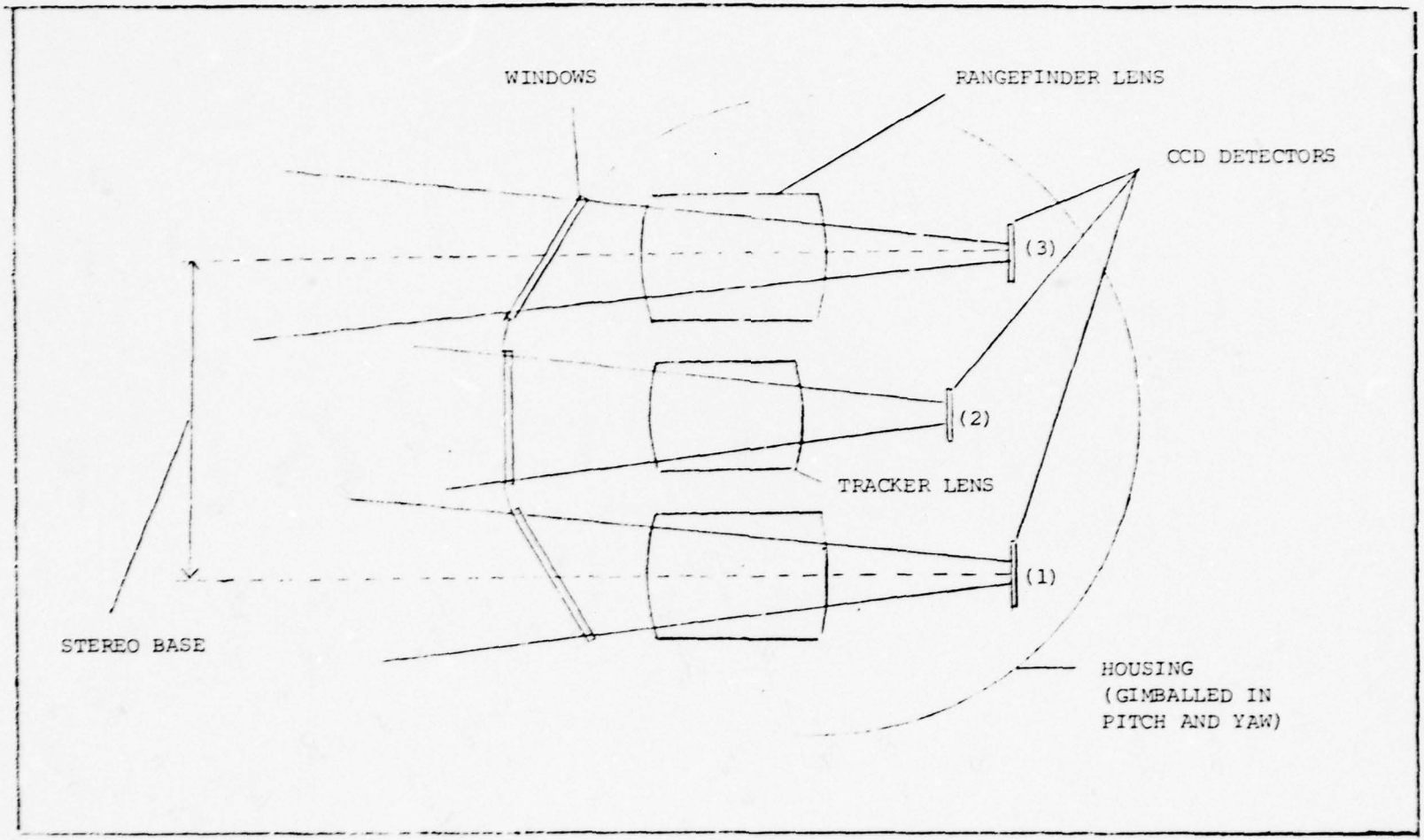

FIGURE 6. Top View Diagram of Proposed Tracker (Ref. 1:2.20)

The range sensors are composed of range lenses and CCD detector arrays. The video signals generated by detector 1 and 3 are used to compute image misregistration between images from two sensors at the same time (Ref 8:2.6). Since they are separated by a baseline, target range can be computed by

$$R = \frac{P}{FB}$$

where P = image misregistration between sensor 1 and 3.

CCD Detectors. The detectors used for the range sensors are Fairchild CCD 211 area arrays. They are metal-oxide-semiconductor (MOS) structures (Ref. 4:38). The semiconductor is doped silicon so that the detector has silicon responsivity (Ref. 8:2.14). The array has 244 elements by 190 elements. The active area of each element is 18 micrometers vertically by 14 micrometers horizontally. Every other column is a vertical analog register used to transport charge packages (see Figure 7). As stated before, the image is focused on this array by a lens system. Each photosensitive element converts the incoming light energy into photo electron-hole pairs. This process is called detection. All the charge carriers, either the electrons or holes, are accumulated at each photosensitive element and are held there by a potential well. They are accumulated for a period of 2.25 ms, called the integration period. At the end of the integration period, all the packages of charge are moved into the vertical registers at one time. Then the packages are moved one step up to the horizontal register. An

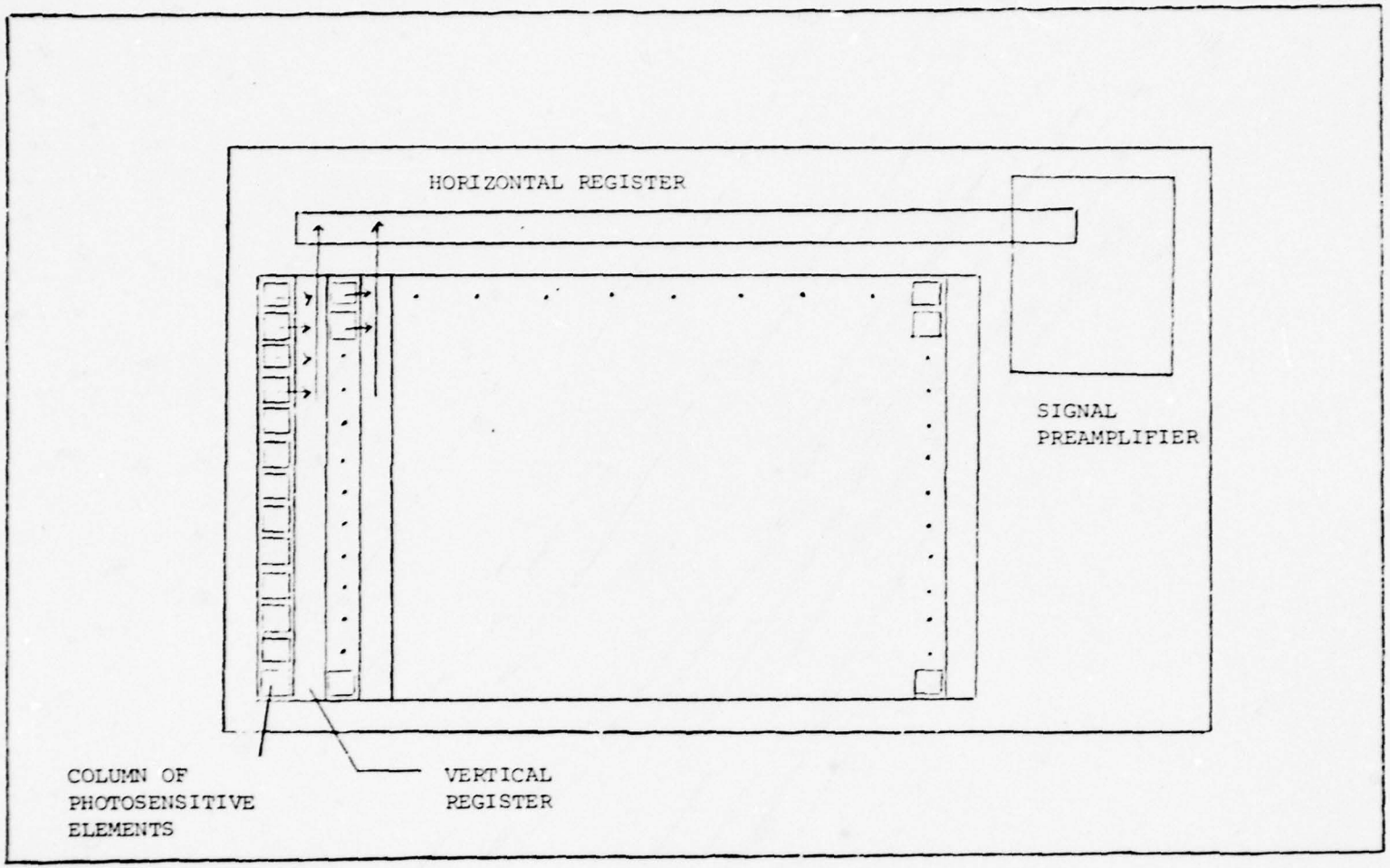

FIGURE 7. Diagram of Fairchild 211 CCD (Ref. 1:2.15)

entire horizontal line of charge packages is transported through a preamplifier which sends the video signal to an amplifier off the CCD chip. Then the vertical registers move all the charge packages up one more increment so that the next line of charge packages is in the horizontal register. The process continues until all the charge packages have been read. In effect, the image is broken down into elements, then these elements are read line by line in the horizontal register (Ref. 9:58). The time it takes to read all the charge packages is referred to as the read-out period. It does not exceed the integration period.

The video signal from the CCD chip is further amplified and then sent to an analog-to-digital converter. The digitized video signal is then sent to the correlation processor. Here, the signal is compared with a previously stored image signal by a correlation algorithm and the image shift is found.

Correlation Algorithm. The correlation function for comparing two scenes is

$$\frac{1}{A} \iint P\ (x,y)\ Q(x + \Delta x,\ y + \Delta y)\ dxdy$$

where

$P\ (x,y)$ = a function representing the target image over the detector surface

$Q\ (x + \Delta x,\ y + \Delta y)$ = a function representing the target image shifted slightly due to an intervening time interval or baseline separation

A = active area of the detector

x and y = the horizontal and vertical directions

The solution of this integral for each possible shift $(\Delta x, \Delta y)$ gives one point of the correlation function. The particular values of $(\Delta x, \Delta y)$ which give a maximum value for the correlation function correspond to the image misregistrations (Ref. 8:II.4).

Recall that the digitized target image has been stored line by line in a memory unit. Two such memories are read out with a delay in one or the other memory. The corresponding elements are multiplied and summed. The resulting number is called the covariance function. The maximum value of the covariance function represents the highest degree of correlation between the image scenes (see Figure 8). The shift which corresponds to the maximum value of the covariance function is the image misregistration. The maximum value is found in one direction, say the x direction, then the image misregistration is found in the other direction by shifting perpendicular to that point.

Several points are computed in each direction. These points can be used to approximate a correlation curve (see Figure 9). The points are run through a correlation algorithm which determines the exact displacement between the two video images (Ref. 8:2.27).

For angular tracking, the two images compared are successive images of the target separated by a time interval. Difference in the two images is assumed to be due to target motion (Ref. 8:2.27). For ranging, the images from sensor 1 and 2 are compared simultaneously. The difference in the two images is assumed to be due to baseline separation. Thus, range can be computed by setting the image

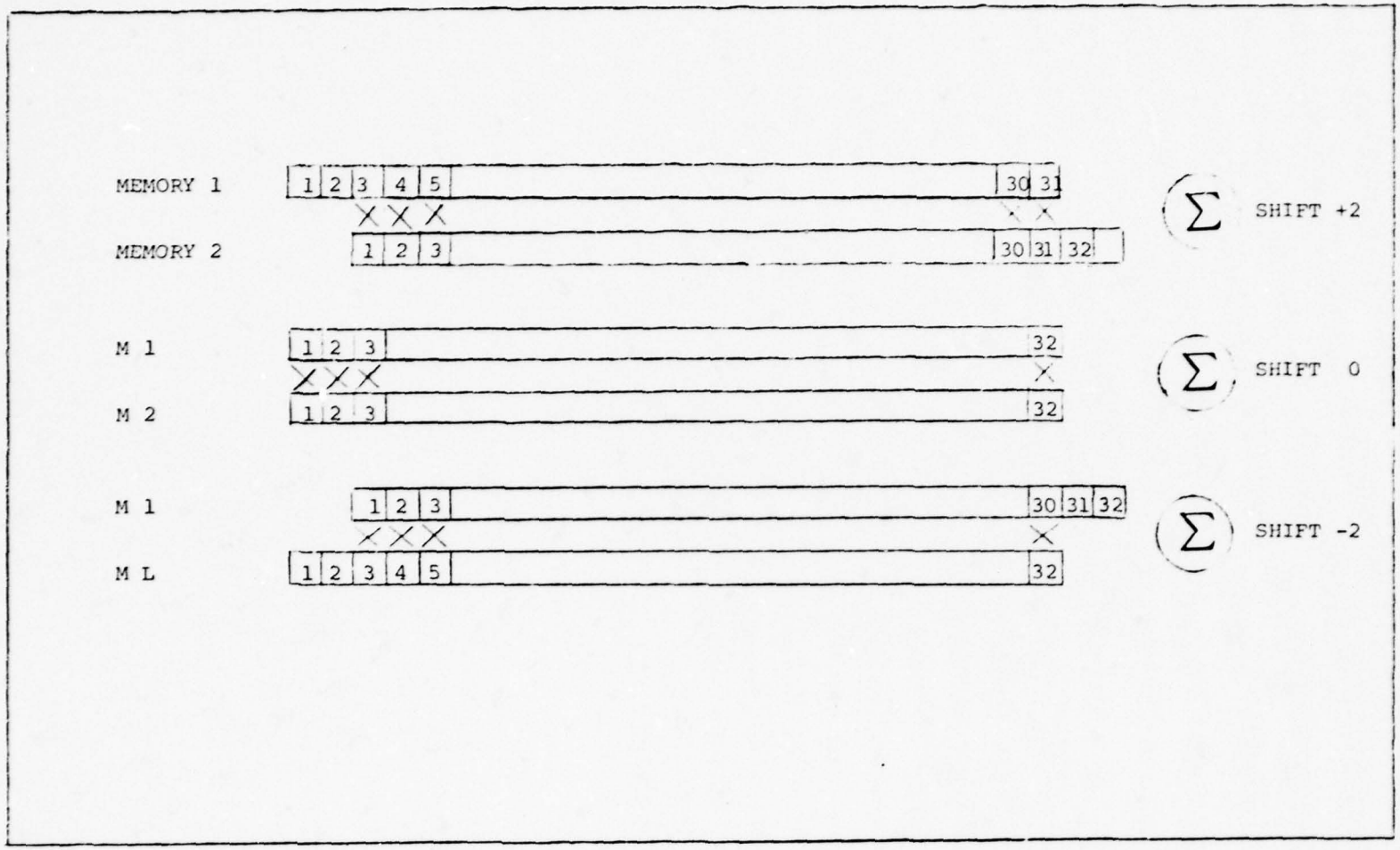

FIGURE 8. Correlation Shift (Ref. 1:228)

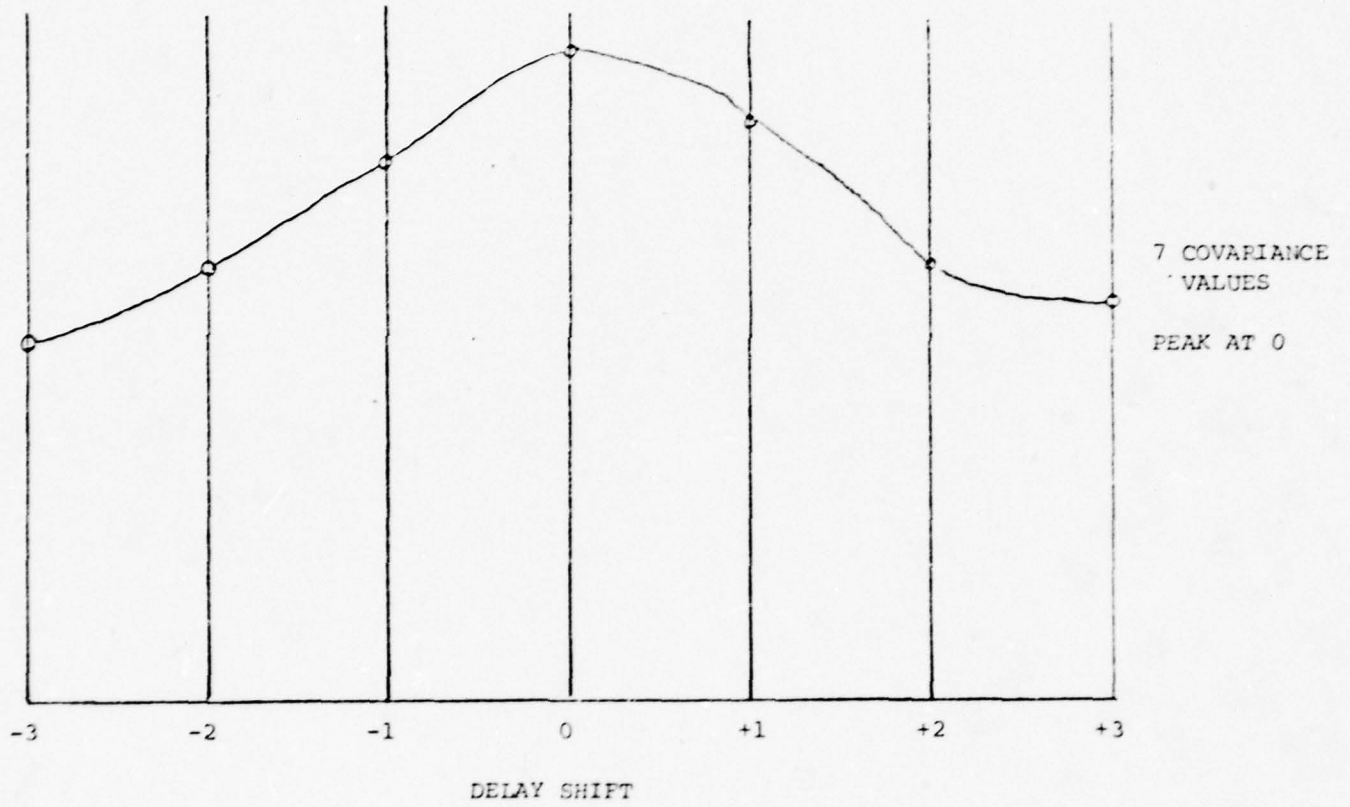

FIGURE 9. Covariance Points on a Correlation Curve
(Ref. 1:2.29)

misregistration equal to the parallax and using Equation (4) to compute the range.

Since the target is moving, the time interval between successive images is important. The smallest time interval possible is the image integration period. For the Fairchild CCD 211, this is 2.25 ms. Signal read-out time is less than integration time so that there is no delay in picking up the next integrated image signal. The additions and multiplications needed to compute the covariance values plus the correlation algorithm also take time to perform. In order for the digital processor to keep up with the image signal generated 450 times every second, the number of photosensitive elements is restricted.

It was found that a sub-area of the array of 8 to 10 elements squared centered on the target was sufficient to perform adequate correlation (Ref. 8:2.34). The maximum number of picture elements allowed will be determined by integration time requirements and necessary update rates for the data. Since the covariance is the sum of the cross multiplication of the picture data, an $n \times m$ array would take $(n \times m)$ multiplications and $(n \times m)$ sums. If the array is increased by one element in either direction, say $(m + 1)$, then there are $(n \times m) + n$ multiplications and sums to be computed for each relative shift. This means that the processor time will exceed maximum detector integration interval if the sub-array exceeds some threshold dimensions (Ref. 8:30).

The data rate required to maintain track on a target or update data to director and weapons release systems are less than 450 Hz. If these rates are 20 Hz (40 samples/sec), then the data being produced

at 450 Hz can be averaged to increase accuracy. A laboratory demonstrator built by CAI has shown resolutions of 1/400 of a photosensitive element at 20 Hz low pass filter break frequency (Ref. 10:I.3-I.4).

Summary

In conclusion for section IV, range accuracy, ΔR , is related to angular resolution of the system. The angular resolution of the system depends on how the video signal is produced and processed. Using a CCD focal plane array and image correlation, CAI Corporation of Bourns Incorporated claims a $\Delta\alpha = \frac{\text{photosensitive element}/400}{F}$. This degree of accuracy is due to the high data rate of the system and assumes a low data rate requirement for tracker servomechanism, aircraft director system and weapons release system.

V. Baseline Separation of Sensors

Introduction

By Equation (6) of Section II, ΔR , the range measurement accuracy, can be improved by increasing the base between the sensors. If the system is to be put on fighter aircraft, the leading edge of the wings provides the widest possible base plus a relatively unobstructed field of view in front of and below the aircraft. A possible exception would be the twin tail booms of the McDonnell Douglas F-15 (Figure 10) and Fairchild-Republic A-10 (Figure 11). Note that the downward view of the sensors will be blocked by the wings in both of these cases. As the primary mission of the A-10 is ground attack, this could seriously limit field of view (FOV). Since the primary mission of the F-15 is air-to-air, the downward FOV is not as important. Table IV shows a comparison of wing spans and tail separation.

Table IV. Comparison of Aircraft

Aircraft	Wingspan	Vertical Tail Separation
A-10	57 ft. - 6 in.	18 ft. - 10 in.
F-15	42 ft. - 9.7 in.	11 ft. - 9 in.
F-16/A/B	31 ft.	----

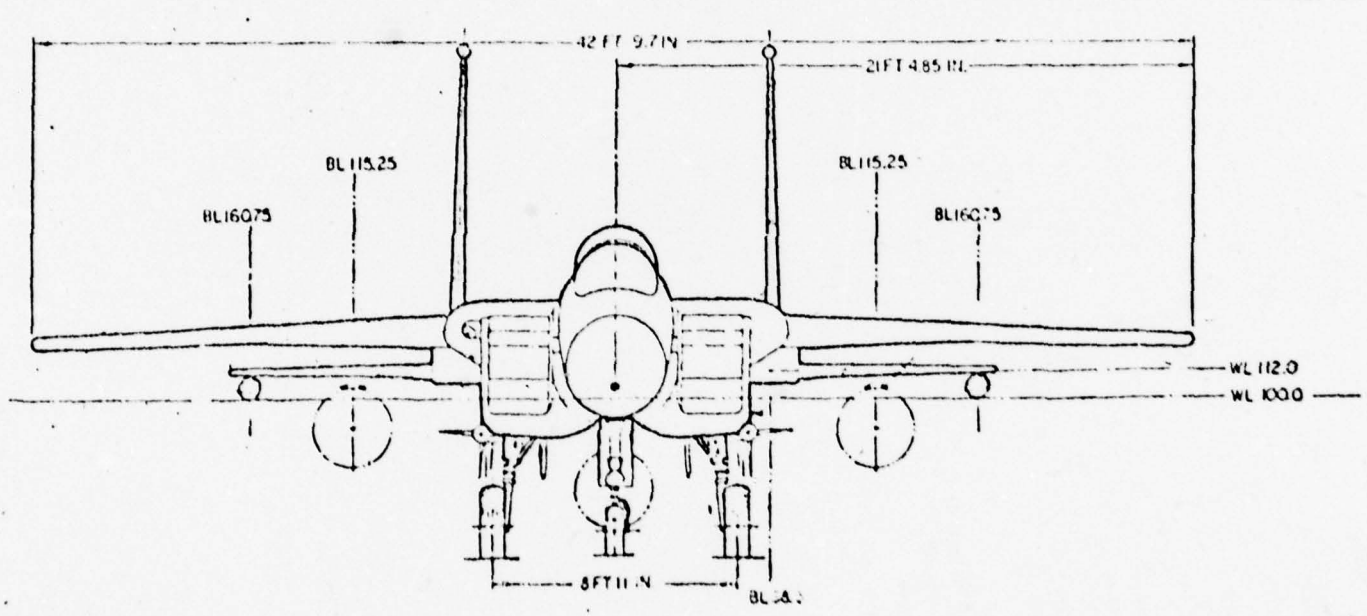

FIGURE 10 F-15

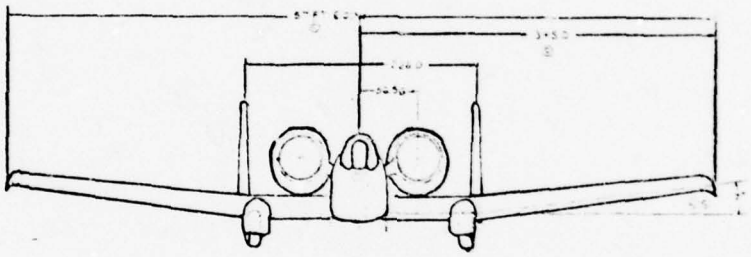

FIGURE 11 A-10

Figure 12 is a graph of maximum range as a function of angular accuracy of the stereo system. The equation used to generate this graph is

$$R_{max} = \frac{(\Delta R/R_{max})B}{\Delta\alpha} \tag{8}$$

$\Delta R/R_{max}$ = the range accuracy desired at maximum range

From Section III, this was .011 .

The target must cover a window of about seven by seven picture elements, pixels, so that an adequate correlation can be performed (Ref. 8:2.34). This is required so that the covariance function can be computed for a shift of ±3 units either side of zero shift. If the target is a small fighter, it will display a cross section as small as one square meter when viewed head-on. The target subtends 6×10^{-6} radians at 89NM in one dimension. In the CCD array, the pixels are spaced every 18 micrometers vertically and 30 micrometers horizontally. In order that the target cover seven of the pixels with 30 micrometers spacing, the optical system must have a focal length of 32.33 meters. One element would have a resolution 4.33×10^{-4} mrad in the horizontal. This is marked on the graph in Figure 12. By insuring that the sensors are spaced by 30 ft, the angular accuracy required of the tracking system is larger than one pixel. In this case, no signal filtering would be required to improve on the image misregistration found by correlation. Using a signal processing to lower $\Delta\alpha$ to 10^{-4} mrad would allow a baseline separation of 5 ft to range accurately out to 89NM.

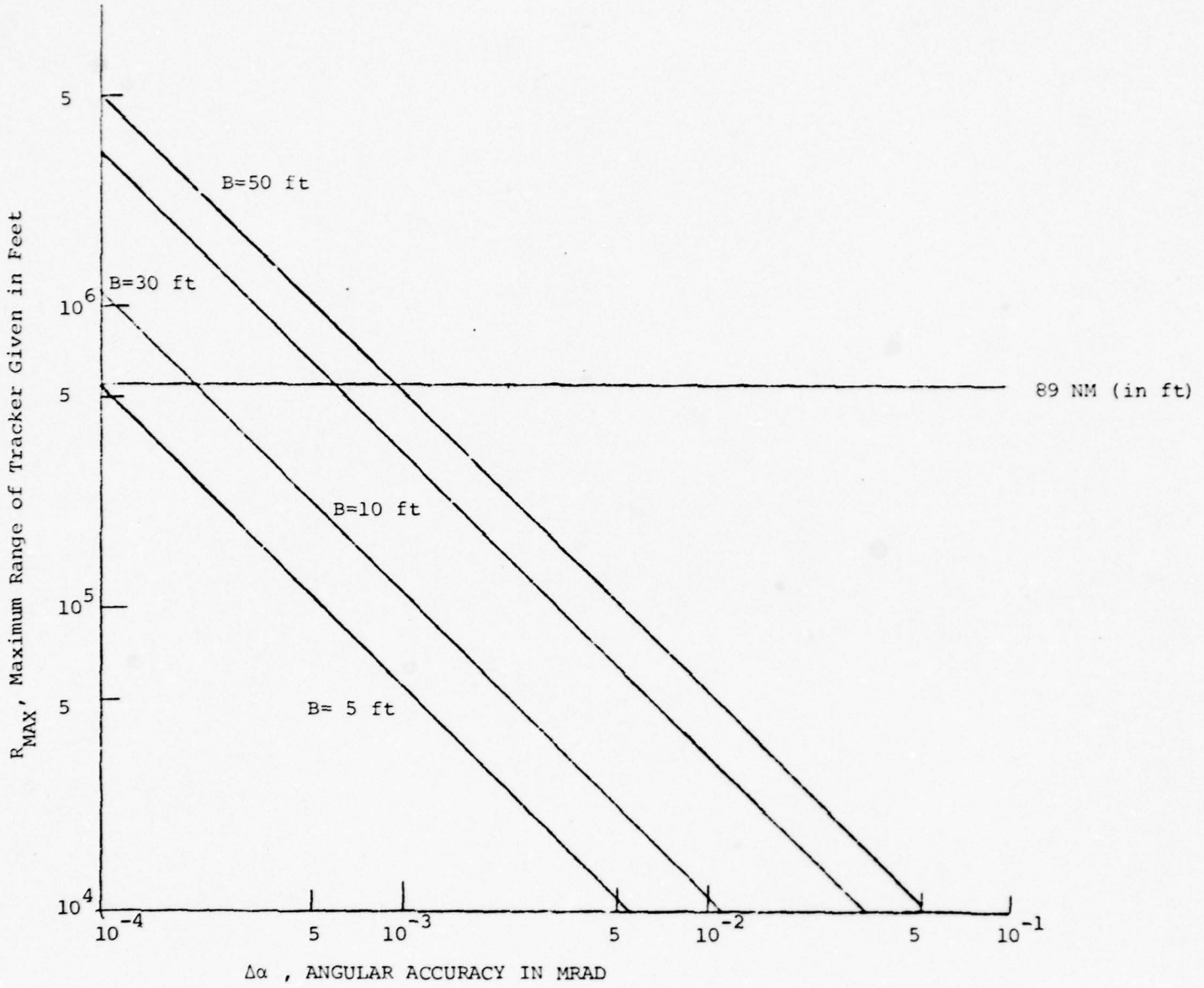

Figure 12. Maximum Range Vs. Δα

Baseline separations of a foot or more will require that the ranging sensors be housed in separate devices. In the unit proposed by CAI, the range sensors optical axes were maintained parallel by means of a solid mount. For split sensors, some other method must be found to keep their optical axes aligned. The alignment must be known to within the accuracy required for ranging, $\Delta\alpha$. Unfortunately, state of the art alignment for remotely located optical systems on an aircraft is only accurate to .1 mrad (Ref 11:8). Determination of a scheme to maintain optical alignment beyond .1 mrad accuracy is beyond the scope of this thesis. From Table III, longest base available is the A-10's 50 ft wingspan. It is apparent from Figure 12 that $\Delta\alpha$ = 1 mrad is required for a base of 50 feet and range of 89NM.

Summary

Maximum range capability using stereometric ranging is related to the baseline in a simple way (Equation (8)). Using a focal plane array and correlation technique described in the CAI proposal requires an optical system with a focal length of 32-1/3 meters. Separating the range sensors to gain a wider base brings out the problem of optical alignment.

Once the ranging sensors have been mounted on the wings, they will be subject to vibrations which will affect their performance. The next section considers the effect of structural vibrations on the sensors.

VI. Effect of Flexure and Vibration on Optical Sensors

Introduction

Aircraft structures, especially the wings and tail, are subject to a number of loads and forcing functions. As a result, they flex and vibrate. Anything attached to these structures are also subject to the effects of flexure and vibration.

Flexure and vibration are terms used to describe two types of elastic motion. Flexure is the elastic bending of a structure due to changes in flight condition (Ref. 11:4). They are low frequency bending. For our purposes, flexures will have a frequency of 5 Hz or less. Vibrations are higher frequency elastic deformations caused by such things as wind gusts, engine vibrations, and flight control motion (Ref. 11:4). For the purpose of this thesis, elastic bending at frequencies higher than 5 Hz is considered to be vibration.

Flexures and vibrations may be classified as linear or angular. When they are linear, they transport the sensor from one position to another in a straight line. When they are angular, they rotate the sensor about an axis.

In the analysis of structural elastic motion acting on the sensors, a coordinate system relative to the sensors and target will be used. The plane containing the two sensors and the target is the sensor-target plane. The direction normal to this plane is the sensor-target normal. The direction from sensor to target is called LOS for line of sight. The last direction is perpendicular to the other two directions and is called LOS perpendicular. Angular vibrations about these three

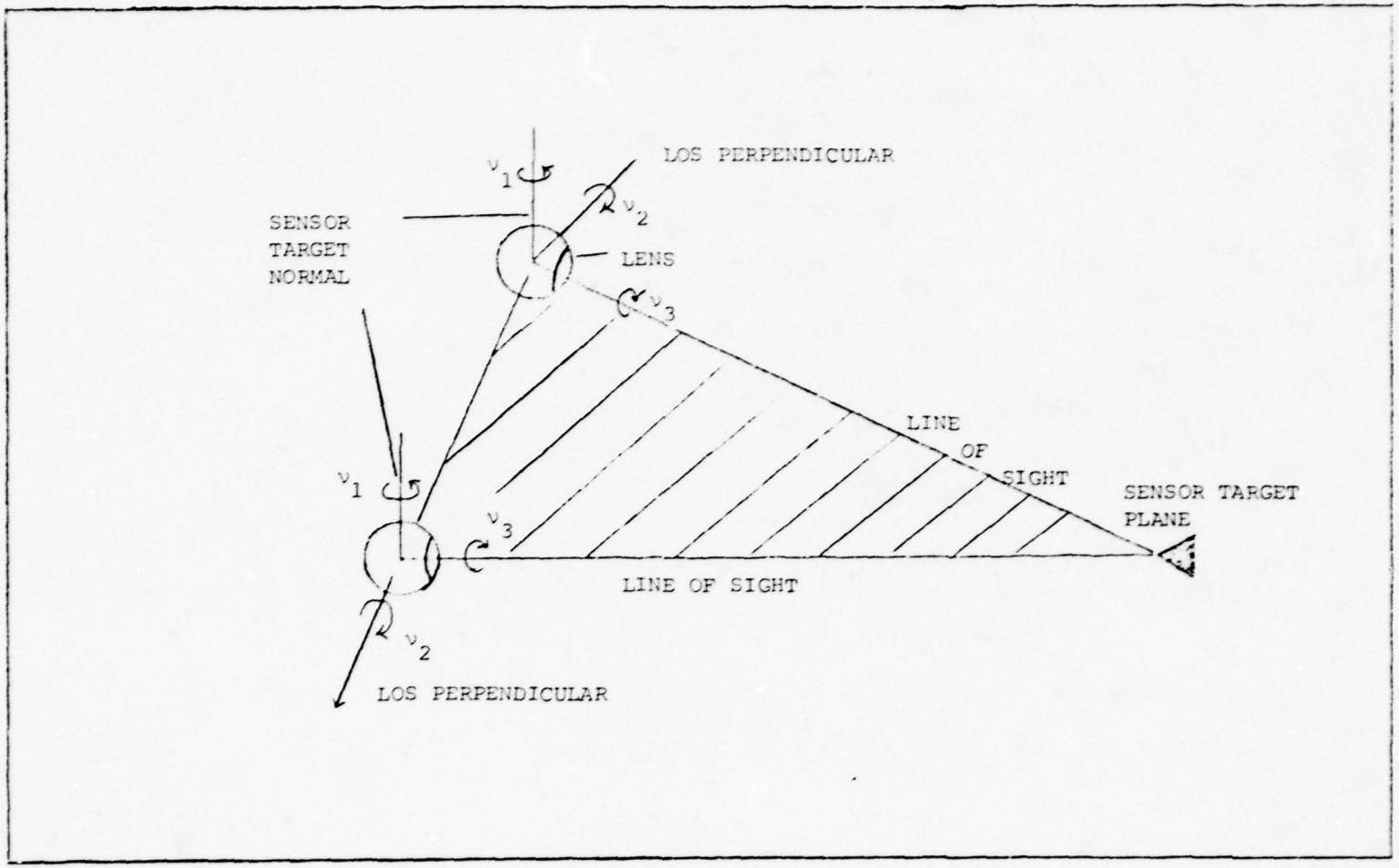

FIGURE 13. Sensor Coordinates

directions will be called ν_1 , ν_2 , ν_3 (see Figure 13). The right hand rule applies.

When analyzing these elastic motions, the effect of their amplitude and rate on the sensor will be considered. Vibrational acceleration affects the sensor mainly through moments and torques on the servomechanisms. Analysis of the servomechanisms is not within the scope of this thesis. The sensors are assumed to be gimbal mounted in elevation and azimuth on the aircraft.

The purpose of this section is to determine the effect of flexure and vibration on focal plane sensors. This effect will be expressed as an equation whenever possible.

Linear Vibrations Effect

Linear vibrational effects are considered first. Their amplitude and rate in each of the three directions result in an interaction with the system which is unique for each direction.

Sensor-Target Normal. In the sensor-target normal direction, vibrational amplitude is measured as changes in target elevation. Both sensors, when they are tracking, point directly at the target. After every integration period, the sensor is corrected via the servomechanisms for any image misalignment found through signal processing. The vibrating sensor indicates that it is the target which is vibrating up and down about an equilibrium position (see Figure 14). Since the sensor measures angles, a displacement in the sensor-target normal is measured as

$$\phi_p = \frac{A_N}{R} \tag{9}$$

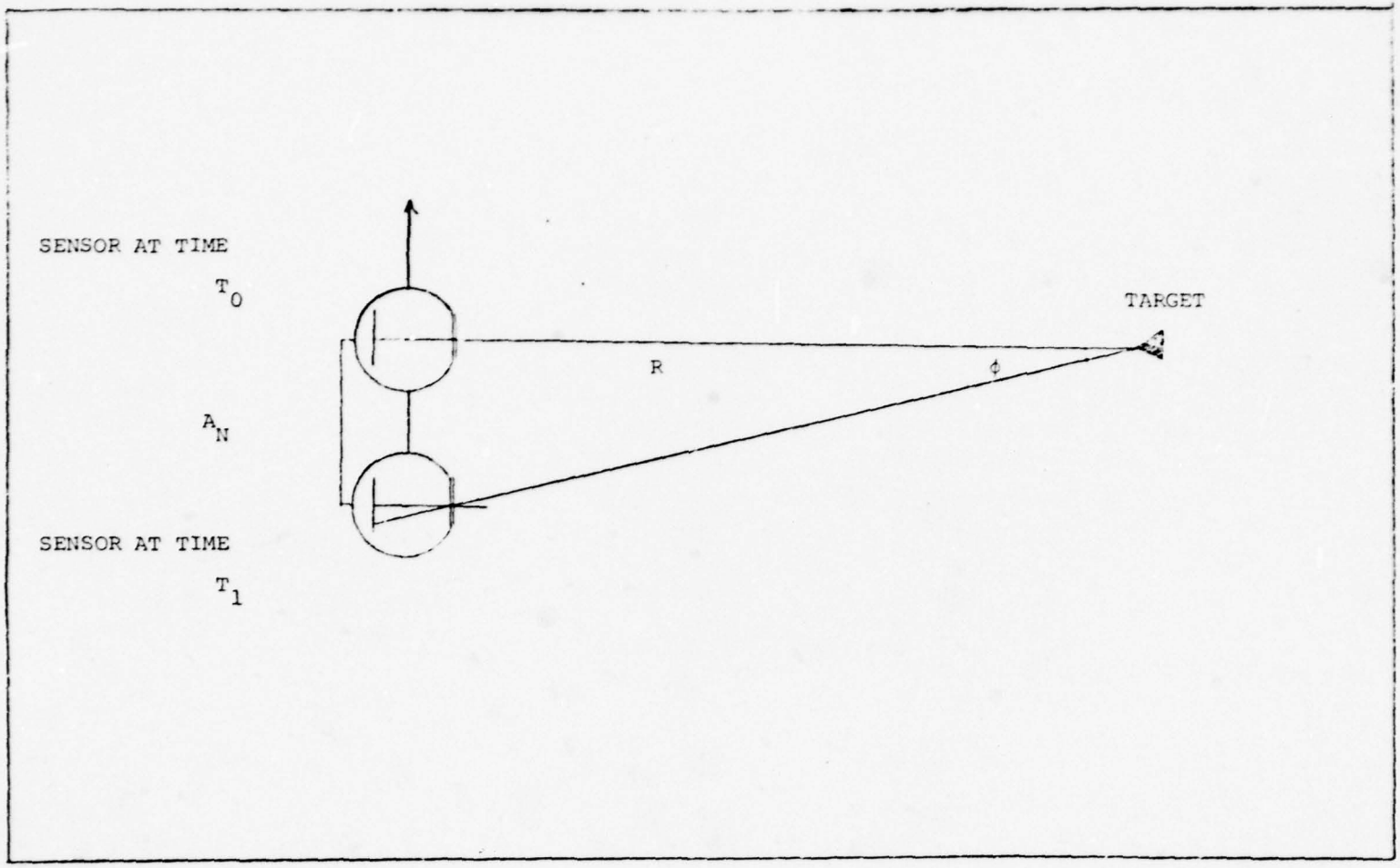

FIGURE 14. Linear Sensor-Target Normal Vibration

where

ϕ_p = angle measured about the LOS perpendicular

A_N = sensor displacement along the sensor-target normal

R = range to the target from the sensor of interest.

This motion has no effect on ranging. The actual elevation angle is found by averaging the elevation signal from the sensor over an interval of time. The averaging can be done in the following manner.

Let

θ_p = elevation angle of the target using the baseline as an axis (Fig. 14a)

Γ = elevation measured by the sensor

$$\theta_p = \Gamma + \phi_p$$

$$\Gamma = \theta_p - \phi_p$$

$$E\{\Gamma\} = \frac{1}{T}\int_{t_0}^{t_0+T} (\theta_p - \phi_p)\, dt' \qquad (9a)$$

$$= \frac{1}{T}\int_{t_0}^{t_0+T} \theta_p\, dt' - \frac{1}{T}\int_{t_0}^{t_0+T} \phi_p\, dt'$$

but

$$\frac{1}{T}\int_{t_0}^{t_0+T} \phi_p\, dt' \simeq 0$$

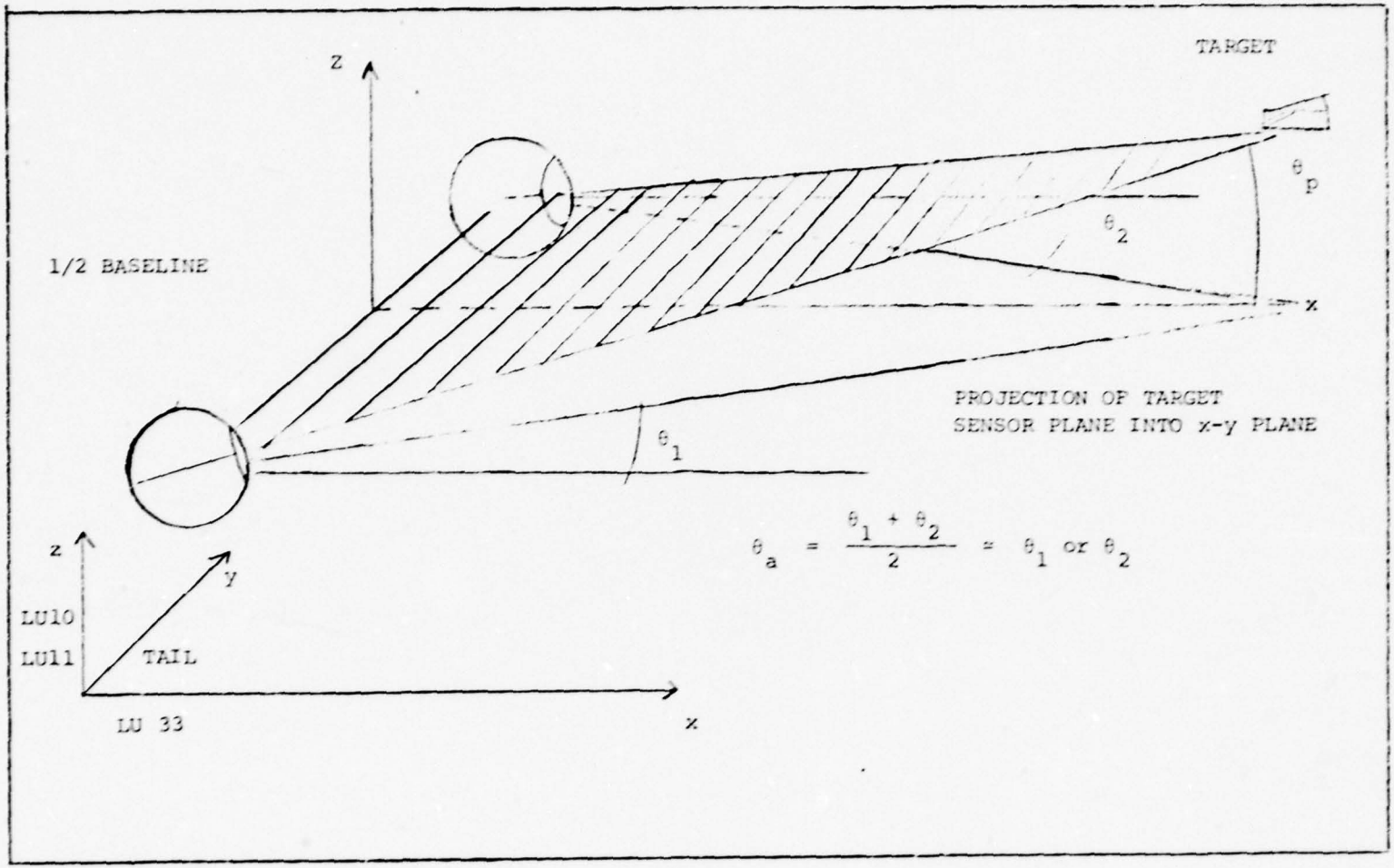

FIGURE 14a. θ_p and θ_a

if $\phi_p(t)$ is a periodic function with a frequency $\omega_v > \frac{1}{T}$

$$E\{\Gamma\} = \theta_p(t_0)\left[\frac{1}{T}\int_{t_0}^{t_0+T} dt'\right] - 0 = \theta_p(t_0)$$

since $\theta_p(t_0)$ = constant over the period T

where

T = an interval of time such that $\frac{1}{\omega_v} < T < \frac{1}{V_{\theta_p}}$

V_{θ_p} = rate at which θ_p changes

ω_v = frequency of the vibration

By averaging the signal, vibrations which go through several oscillations in time T have an average value close to zero. For the purpose of this thesis, vibrations with a frequency of $\omega_v = \frac{2}{T}$ are assumed to be averaged to zero. Vibrations below frequency ω_v will be averaged together to determine the mean amplitude and rate for the vibrating structure.

The vibration can be thought of as a composite of vibrations with a continuous distribution of frequencies. In theory, this distribution of frequencies goes from 0 to ∞. In reality, however, the data collected on these vibrations only cover the range 5 to 1000 Hz. The lower limit is due to the inability of the sensors to measure vibrations accurately below that frequency. The upper limit is observed empirically from the data.

The maximum value for T is important, since it determines ω_v.

The maximum value for T is limited by the assumption that θ_p is a constant during T. In Table III, the LOS angular accuracy, $\Delta\theta_{LOS}$, is specified to be a maximum of 1 mrad. θ_{LOS}, the LOS angle to the target, is a combination of the target's elevation and azimuth angles. If the azimuth angle is suppressed for this analysis, $\theta_{LOS} = \theta_p$. Likewise, $\Delta\theta_p \approx \Delta\theta_{LOS}$ and $\dot{\theta}_p = \dot{\theta}_{LOS}$. If $\dot{\theta}_p$ is is the rate at which the target's elevation angle changes, then $T = \Delta\theta_p/\dot{\theta}_p$. The rate at which θ_p changes depends on several factors, such as the type of target, its velocity, and its range. Of the two basic types of missions, air-to-air and air-to-ground, the air-to-ground mission usually involves the highest rates for θ_p.

For example, if a fighter makes a level bomb run on a ground target (Fig. 14b)

$$\dot{\theta}_p = \frac{V_f \sin \theta_p}{R^2}$$

Assume $\sin \theta_p = \frac{A}{R}$

then $\dot{\theta}_p = \frac{V_f A}{R}$

where

V_f = velocity of the fighter

A = fighter's altitude above the target

R = slant range to the target

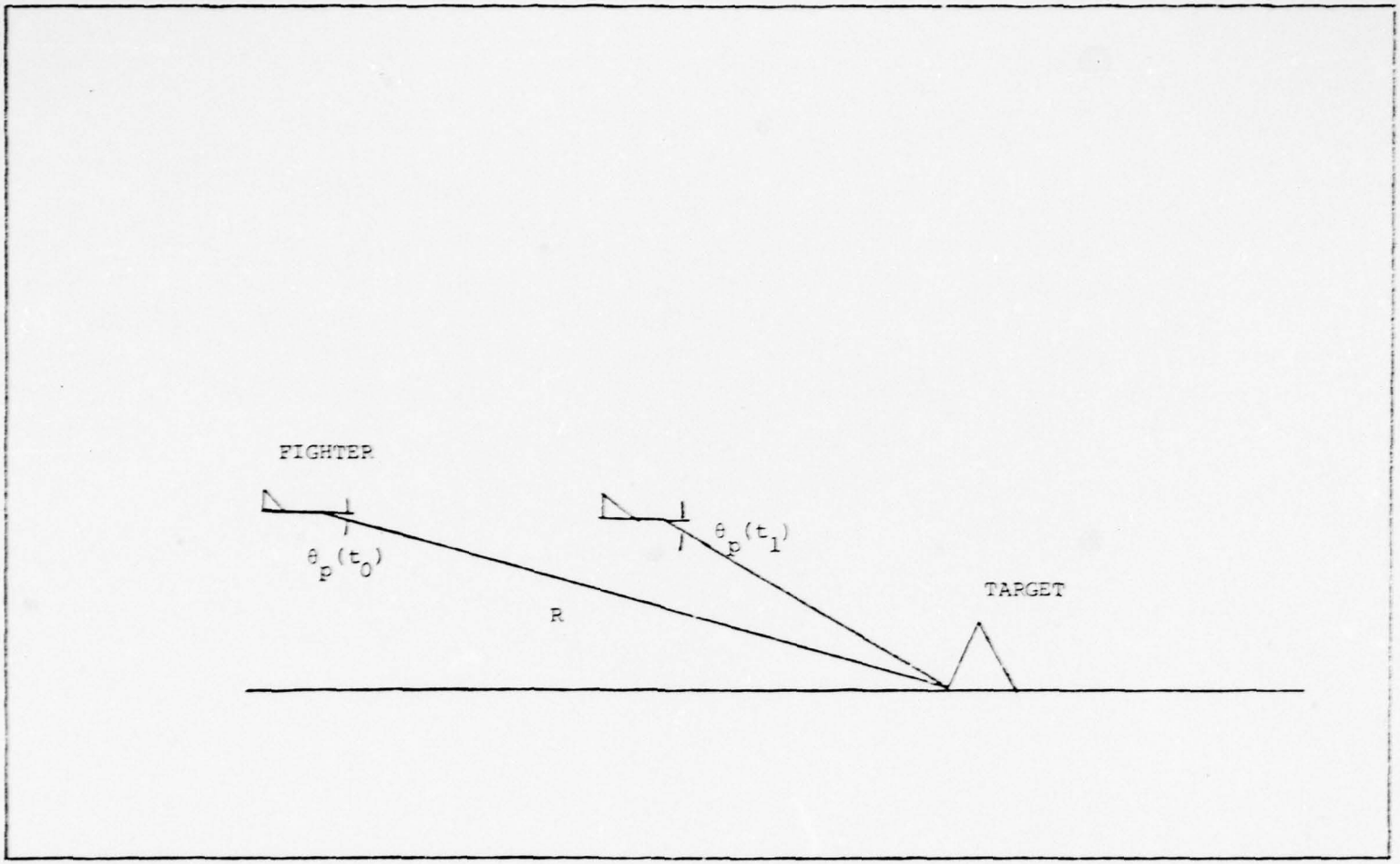

FIGURE 14b. θ_p for Level Bomb Run

$$T = \frac{\Delta\theta_p}{\theta_p} = \frac{\Delta\theta_p R^2}{V_f A} \tag{9b}$$

Figure 14c is a graph of Equation (9b). The two curves plotted in Figure 14c represent two different fighter velocities. The approximate release ranges based on bomb time of fall and fighter altitude are marked by vertical lines. The value of T corresponding to these ranges are marked with horizontal lines. Since $\omega_v = \frac{2}{T}$, $\omega_v = 71$ Hz for R 7000 ft and $\omega_v = 95$ Hz for R 5000 ft. A_n is found by averaging the amplitudes of the vibrations from 5 Hz to ω_v. Therefore, it is necessary to locate the sensors at a position where A_n is no greater than

$$\frac{A_n}{R_n} = \phi_p = \Delta\theta_p \tag{10}$$

where

R_n = minimum range capability of the tracker.

Minimum range is used to calculate A_n because it puts the greatest restriction on A_n.

Vibrational rate has another effect on sensor accuracy. During the integration period, the target is smeared over the detector array. The amount of smear is equal to the vibration rate times the integration period times the focal length, all divided by the range. Image smear affects sensor pointing accuracy by distorting the video signal. The relationship between image smear and pointing accuracy could be determined by experimentation. The experiment would consist of increasing

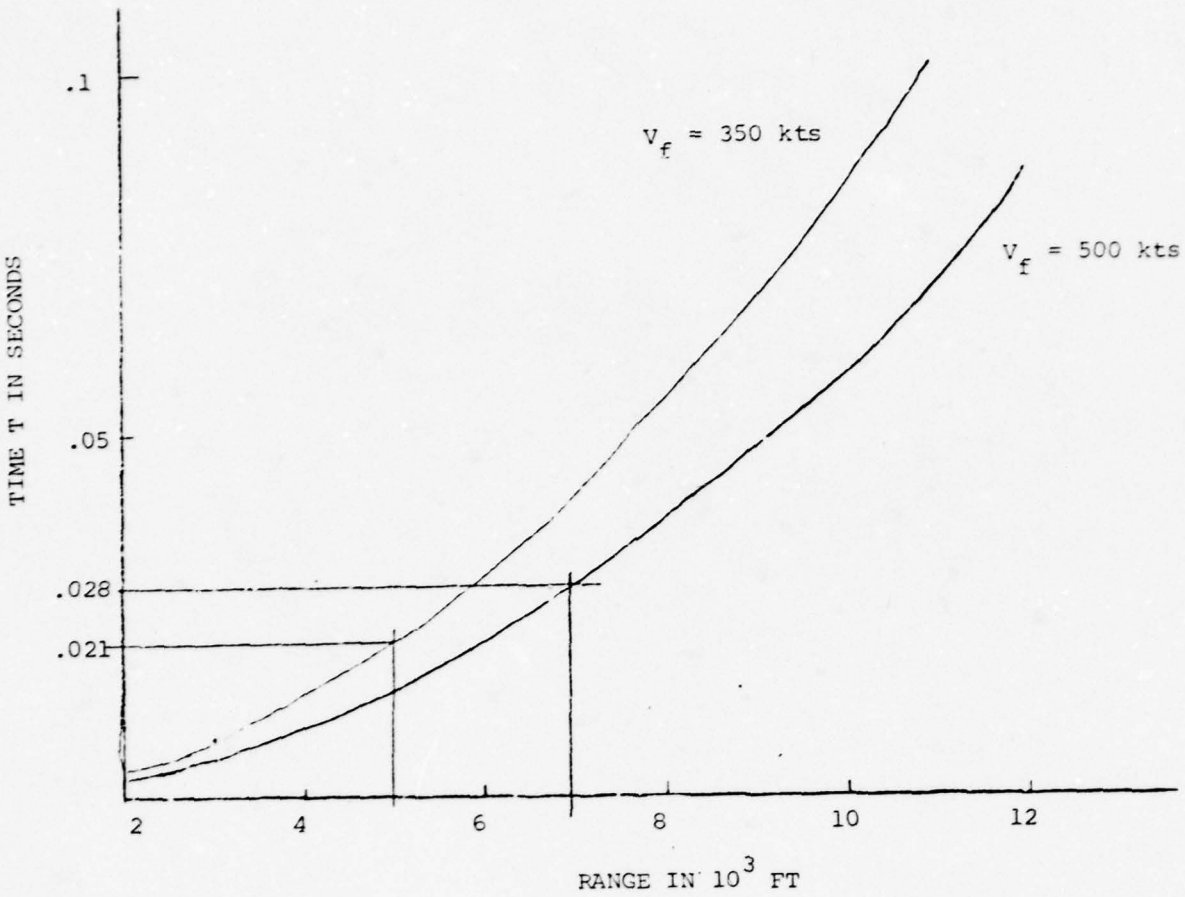

FIGURE 14c. T Vs. Range for Bomb Run

the rate of vibration while observing pointing accuracy. Given a required pointing accuracy, the threshold for image smear would be set. If this threshold is represented by σ_{LT} , then

$$\dot{A}_N = \frac{\sigma_{LT} R_n}{t_i F} \tag{11}$$

where

$\dot{A}_n$ = maximum allowable linear vibration rate along the sensor-target normal

t_i = integration period for detector

LOS Perpendicular. Linear vibrations in this direction affect each sensor's measurement of the target's azimuth. Amplitude of the vibration is measured as an angle, just as it is for the sensor-target normal direction. Similar to Equation (9)

$$\sigma_a = \frac{A_p}{R} \qquad \text{(Ref. Fig. 15)} \tag{12}$$

where

σ_a = angle measured about the sensor-target normal

A_p = amplitude of vibration in the LOS perpendicular direction

Similar to Equation (9a), the true azimuth angle could be found by averaging the signal over a period of time, T . Since $\omega_v = \frac{2}{T}$, the vibrations above ω_v will not affect the measurement of θ_a , the azimuth angle of the target measured from the fighter's longitudinal axis.

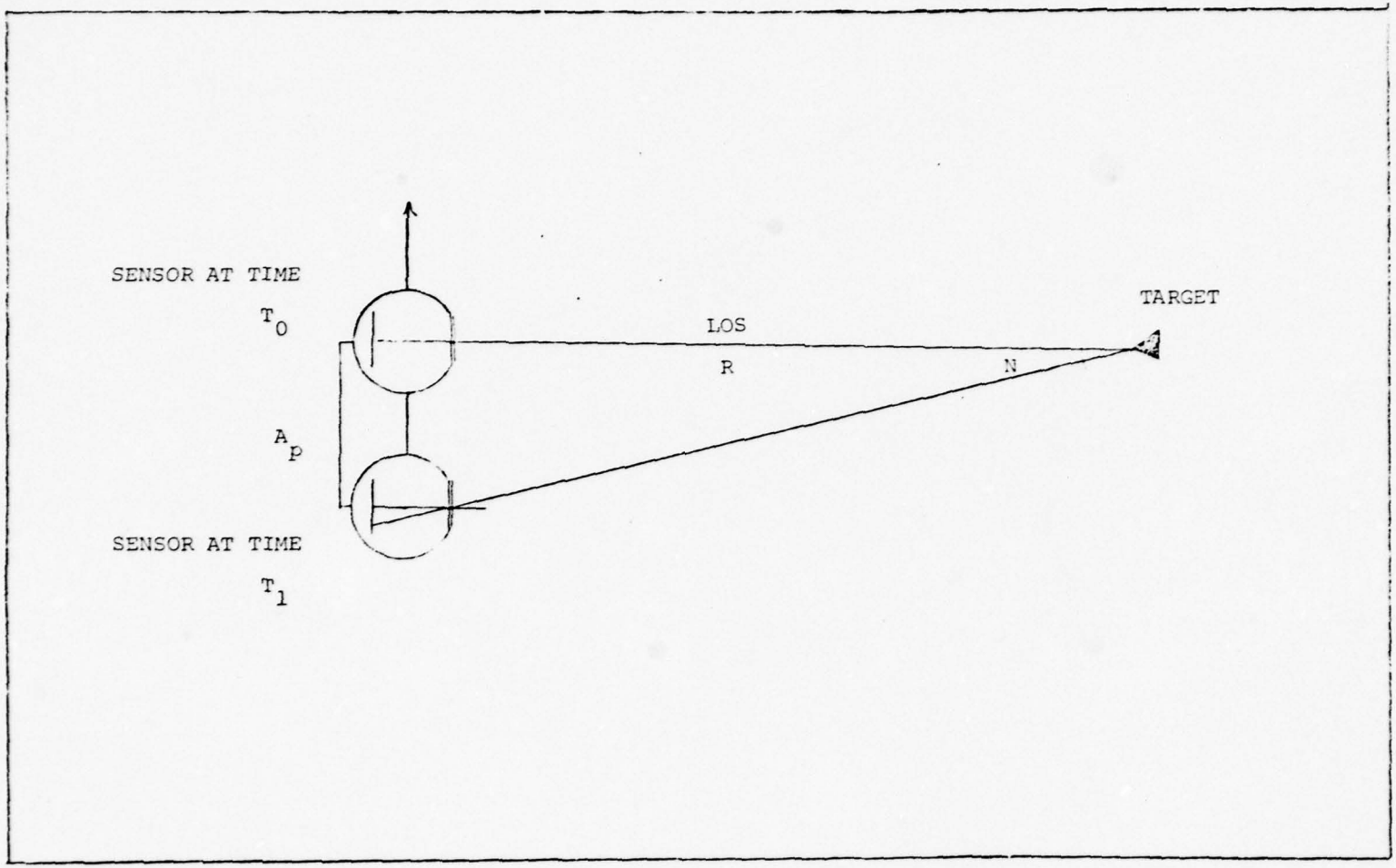

FIGURE 15. Linear LOS Perpendicular Vibration

When measuring θ_a , the maximum value of T is limited by the assumption that θ_a is a constant during T . If it is desired to measure θ_a to 1 mrad (Table III) and $\dot{\theta}_a$ is known, then

$$T = \frac{\Delta\theta_a}{\dot{\theta}_a} \tag{12a}$$

$\dot{\theta}_a$, just like $\dot{\theta}_p$, depends on many factors such as type of target and mission. Of the two basic missions, air-to-air and air-to-ground, air-to-air missions usually produce the greatest values for $\dot{\theta}_a$.

For example, if a fighter performs an intercept on another aircraft, the θ_a can reach values which significantly limit T . An intercept can be broken into three phases, based on range. The initial phase of the intercept extends from initial range to about 10 NM. This phase of the intercept is characterized by very low $\dot{\theta}_a$. This is because the fighter maintains the target at the θ_a which would cause them to eventually collide. This θ_a does not change at all as the two aircraft approach each other. The conversion phase of the intercept occurs in the ten to two nautical mile range. During this phase of the intercept, the fighter maneuvers from a head-on attack to a stern attack. This phase of the intercept is characterized by relatively high values for $\dot{\theta}_a$. The final phase of the intercept occurs from two nautical miles down to minimum range. The fighter chases the target down during this phase. The angular LOS rate is very low here also, and his little effect on T .

During the conversion phase of the intercept, the fighter usually executes a pure pursuit curve. If this is the case,

$$\dot{\theta}_a = \frac{V}{R}$$

where

V = velocity of the target perpendicular to the LOS

R = range to the target

V for a pure pursuit curve is given by

$$V = V_{tgt} \sin \theta_{asp}$$

where

V_{tgt} = target's velocity

θ_{asp} = target's aspect angle.

The aspect angle is an angle determined by the target's longitudinal axis and the LOS from the fighter to the target (Ref. Fig. 15a). The aspect angle increases from $0°$ to $180°$ as the fighter converts to the target's stern. Again, assuming the fighter executes a pure pursuit path as it converts to the stern, θ_{asp} may be approximated by

$$\theta_{asp} = \left(\frac{180°}{8 \text{ NM}}\right)\left(R - 2 \text{ NM}\right) \quad , \quad 2 \text{ NM} \leq R \leq 10 \text{ NM}$$

Since $T = \frac{\Delta\theta_a}{\dot{\theta}_a}$

then

$$T = \frac{.1 \text{ mrad } R}{V_{tgt} \sin[\frac{180°}{8}(R-2)]} \tag{12b}$$

A plot of this function shows that $T \approx .04$ seconds from 3 to 6 nautical miles (see Fig. 15b). Therefore, vibrations of frequencies

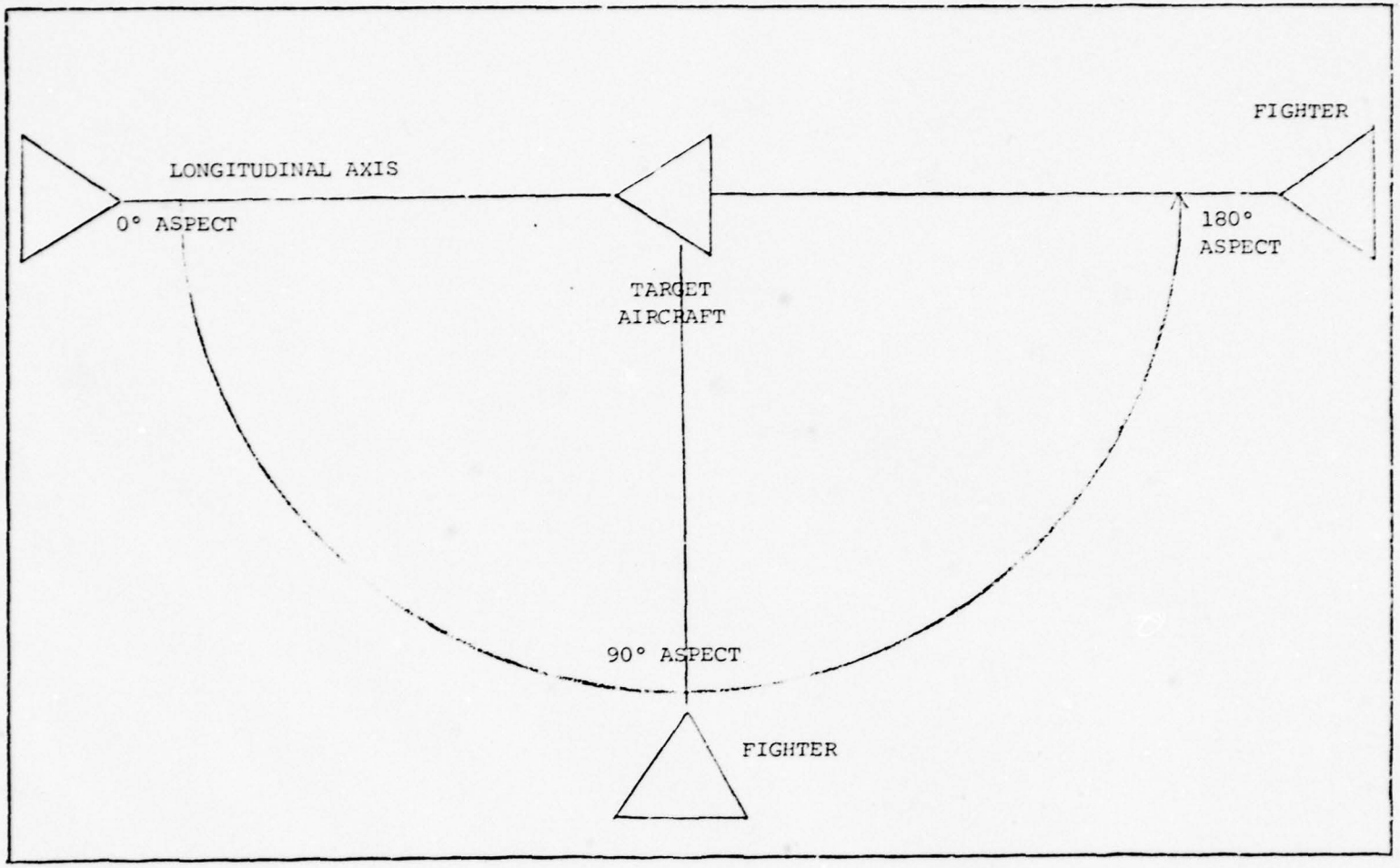

FIGURE 15a. Aspect Angle

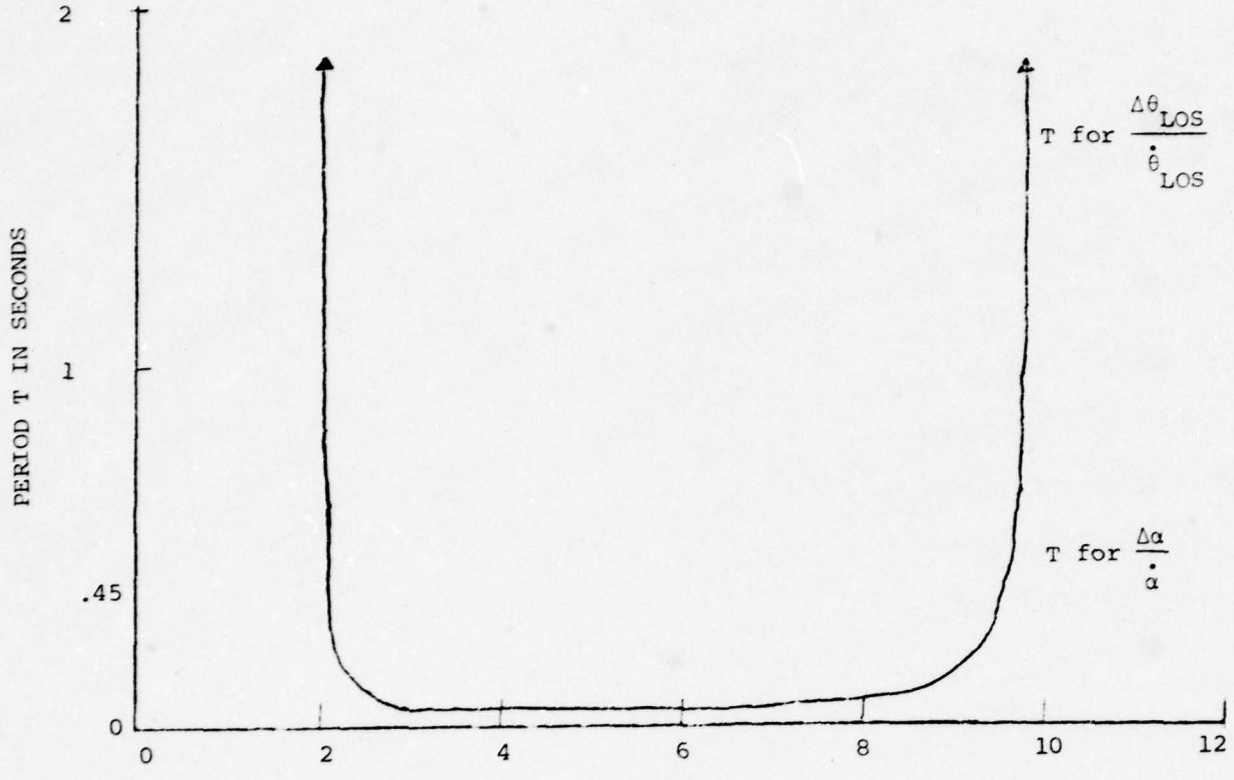

Figure 15b. Range in Nautical Miles

5 to 50 Hz will contribute to the mean value for A_p . Similar to Equation (10),

$$\frac{A_p}{R_n} = \phi_a = \Delta\theta_a \tag{12c}$$

The amplitude of vibrations in the LOS perpendicular direction also affects the stereometric tracker's range measurement. The tracker measures target range by computing the difference in target azimuth measured by the two sensors (Fig. 4). ϕ_a is measured by each sensor as part of the azimuth angle to the target. Figure 16 represents two sensors mounted on a wing which is subject to vibrations. Sensor 2 is allowed to do all the vibrating while sensor 1 is steady. In effect, ϕ_a is the sum of the angular deflection due to both sensors. Φ is the difference between θ_1 and θ_2 (see Fig. 4). From Fig. 16 it can be seen that

$$\Phi = (\alpha - \phi_a)$$

$$R = R(\Phi) = R(\alpha - \phi_a)$$

$$\frac{R}{B} = \text{ctn}\ \Phi \simeq \frac{1}{\Phi}$$

The last equality uses the small angle approximation.

$$R = \frac{B}{\Phi} = \frac{B}{(\alpha-\phi_a)} \tag{13}$$

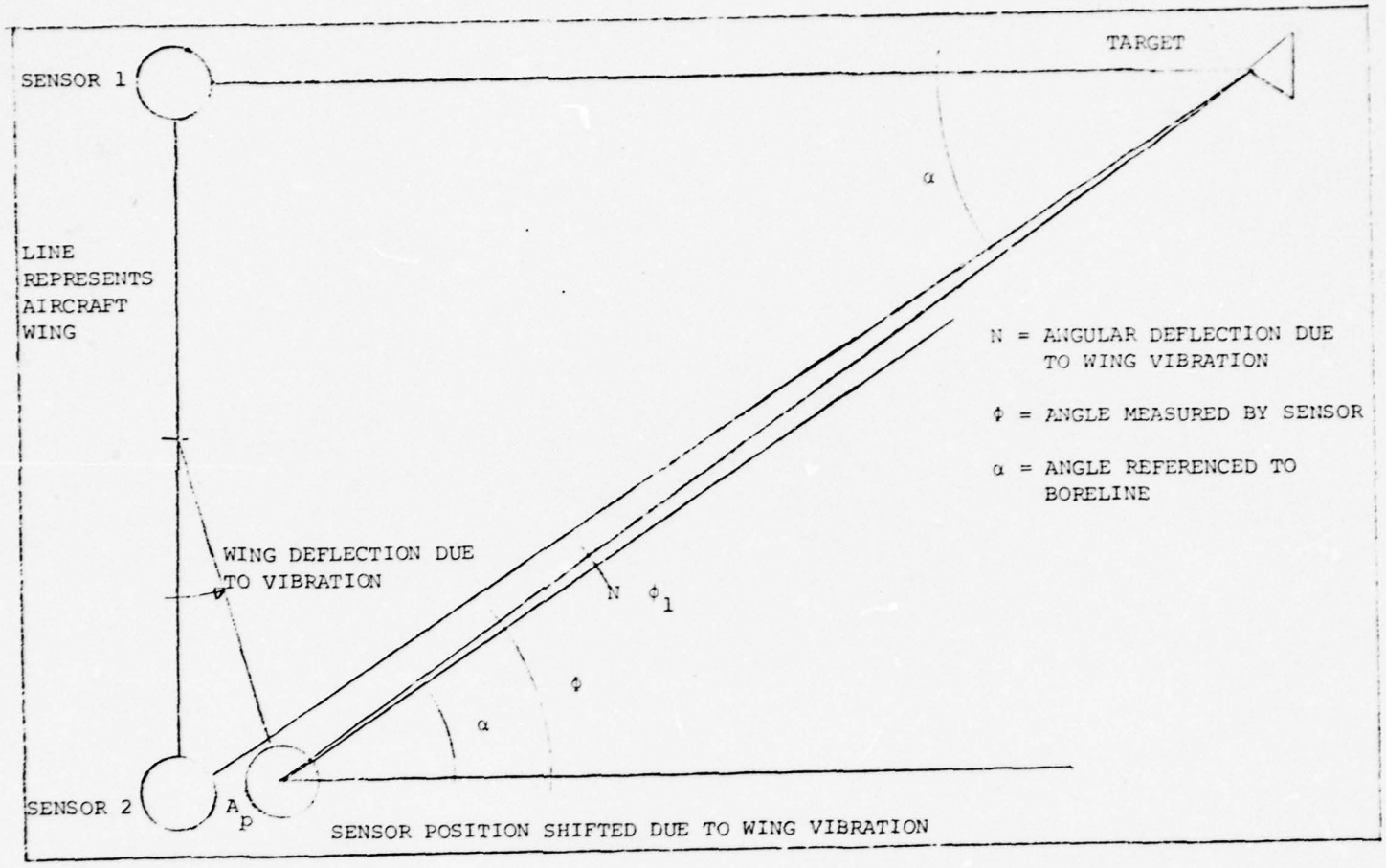

FIGURE 16. Diagram of Sensors on Aircraft Wing

If the angular deflections due to vibration are assumed to be small compared to α ,

$$R = \frac{B}{\alpha}\left(1 + \frac{\phi_a}{\alpha} + \left(\frac{\phi_a}{\alpha}\right)^2 + \ldots\right)$$

$$\simeq \frac{B}{\alpha}\left(1 + \frac{\phi_a}{\alpha}\right) \tag{14}$$

If

R_a = actual range to the target = $\frac{B}{\alpha}$

then

$$R = R_a\left(1 + \frac{\phi_a}{\alpha}\right) \tag{15}$$

where

$\frac{\phi_a}{\alpha}$ represents a percentage of the range error.

Since the sensors are mounted on an aircraft moving through the air, α is a function of time. It is a slowly varying function of time compared to ϕ_a . An average or expected value of R , $E\{R\}$, is given by

$$E\{R\} = \frac{1}{T'}\int_{t_0}^{t_0+T'} R(t')\, dt' \tag{16}$$

where a period T' is such that

$$\frac{1}{\omega_v} > T' > \frac{1}{V_\alpha}$$

ω_v = frequency at which the sensor is vibrating

V_α = rate at which α is changing

Then

$$E\{R\} = \frac{1}{T'} \int_{t_0}^{t_0+T'} R_a(t') \left(1 + \frac{\phi_a(t')}{\alpha(t')}\right) dt'$$

$$= \frac{1}{T'} \int_{t_o}^{t_0+T'} R_a(t')\, dt' + \frac{1}{T'} \int_{t_0}^{t_0+T'} \frac{R_a(t')}{\alpha(t')} \phi_a(t')\, dt'$$

From the assumption on T, $R_a(t)$ and $\alpha(t)$ can be considered to be constants over the integration.

Thus

$$E\{R\} \simeq R_a(t_0) + \frac{1}{T'} \frac{R_a(t_0)}{\alpha(t_0)} \int_{t_0}^{t_0+T'} \phi_a(t')\, dt'$$

But

$$\int_{t_0}^{t_0+T'} \phi_a(t')\, dt' \cong 0 \qquad (16a)$$

Since ϕ_a is a periodic function with frequency $\omega_v > \frac{1}{T}$.

Thus

$$E\{R\} = R_a \qquad \text{(Ref. 12)}$$

The upper limit on the period of time, T, over which $E\{R\}$ is averaged is set by the assumption that $R_a(t)$ and $\alpha(t)$ are constants. In actuality, $\alpha(t)$ has a rate which can be expressed in terms of range, R, as

$$\dot{\alpha} = \frac{B}{R^2} V_c$$

where

$\dot{\alpha} = \frac{d\alpha}{dt}$

V_c = rate at which the target and fighter are closing

The accuracy to which α is known, $\Delta\alpha$, can also be expressed in terms of range:

$$\Delta\alpha = \left(\frac{\Delta R}{R}\right) \frac{B}{R} = C \frac{B}{R}$$

where

R = desired range accuracy

$\left(\frac{\Delta R}{R}\right)$ = a constant for all ranges

The upper limit for T is found from

$$T = \frac{\Delta\alpha}{\dot{\alpha}} = \frac{C}{V_c} R \qquad (16b)$$

If the target is another aircraft with a velocity of 500 kts and the fighter, also at 500 kts, is attacking head-on, V_c is 1000 kts. If $\Delta R/R$ = 1.1 NM/89 NM = .0125 is made a constant for all ranges, Equation (16b) becomes

$$T = (4.5\ 10^{-2}\ \frac{\text{sec}}{\text{NM}})\ R \qquad (16c)$$

Figure 15a is a graph of this relationship. For a ground target V_c = the fighter's velocity, Equation (16c) becomes $T = (.09\ \frac{\text{sec}}{\text{NM}})\ R$.

The linear relationship between T and R assumes the fighter maintains the same aspect to the target during the attack. If the fighter is attacking another aircraft, the crew may want to convert from a frontal attack to a stern attack. For the example of a fighter attacking a target head-on with a V_c of 1000 kts, the crew should start a conversion to the target's stern around ten nautical miles. The crew will try to maintain $V_c = (100\ \frac{\text{kts}}{\text{NM}})\ R$ as they convert to the target's stern by 2 NM and then continue to close to minimum range. Using the relationship in Equation (16b)

$$T = \frac{C}{100\ \text{kts}} = .45\ \text{seconds} \qquad (16d)$$

For the case in which the fighter performs a frontal attack to a missile launch, the crew may want the ability to track accurately down to minimum launch range of the missile. If the minimum range is approximated by 10% of the maximum range, then Equation (16c) gives

$$T = .09\ \text{seconds}$$

for a 20 NM missile.

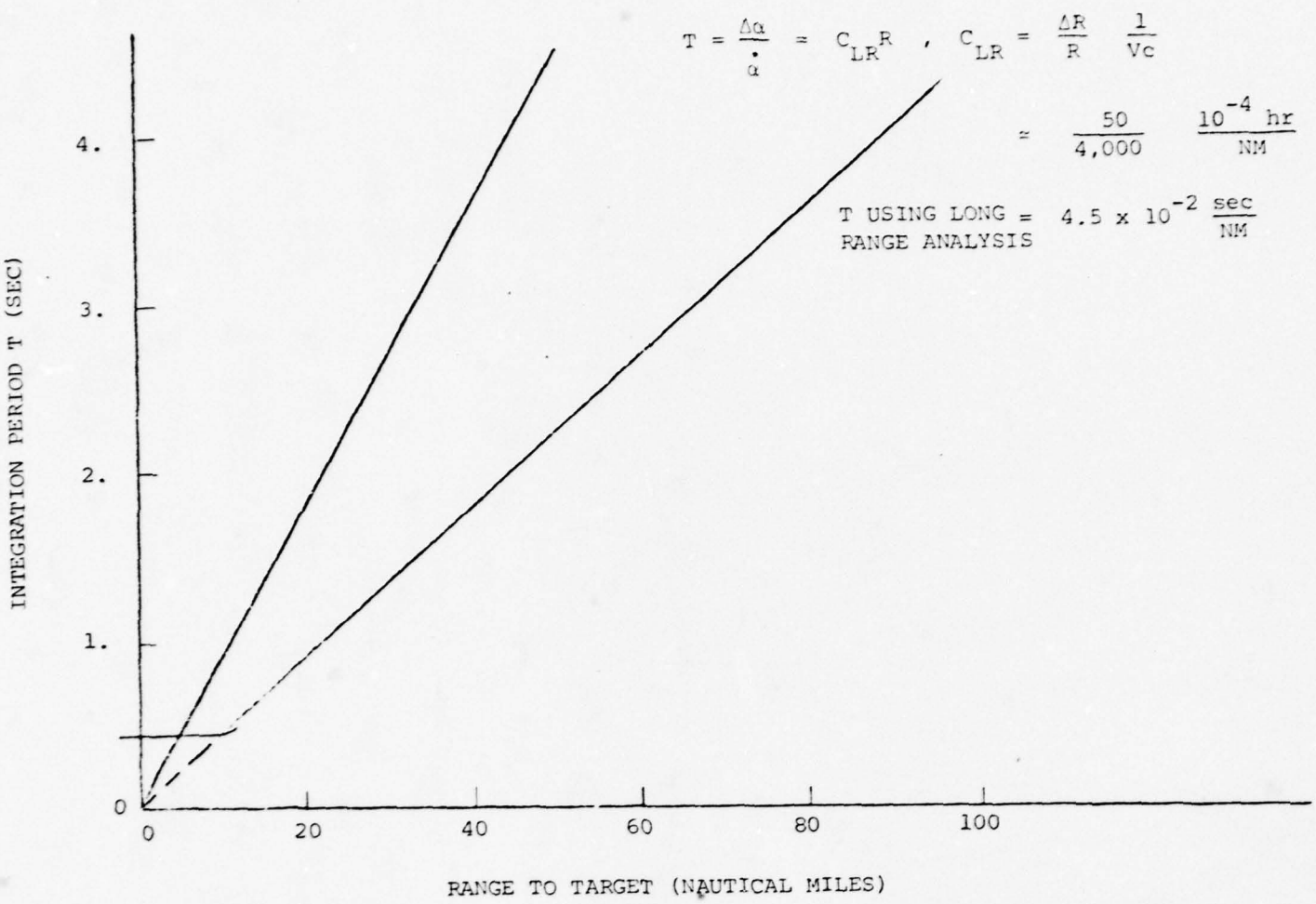

FIGURE 16a. T Vs. Range for Constant Azimuth

Since $\omega_v = \frac{2}{T}$, $\omega_v = 5$ Hz for a frontal attack. In either case, the amplitudes of the vibrations from 0 to ω_v will contribute the mean value of A_p . The position at which the sensor is placed will have to be such that

$$\sqrt{2}\ \frac{A_p}{R} \leq \Delta\alpha = \left(\frac{\Delta R}{R}\ \frac{B}{R}\right) \tag{17}$$

Comparing the graphs of Figure 15b and 16a shows that T is limited by Equation (16b) down to ranges of 10 NM. If the crew converts to the stern using a pursuit curve, Equation (12b) yields the greater limitation on T . During the final phase of a stern attack, Equation (16d) is valid. These equations will be used in Section VII to determine the upper frequency limit of the vibrations which will influence the performance of the optical tracker. However, if one considers that the sensors are held on target by rate servomechanisms, it is possible to use even longer integration time intervals than computed in these equations. The rates $\dot{\theta}_a$, $\dot{\theta}_p$ and $\dot{\alpha}$, are relatively constant. The rate at which the servos correct the sensor's optical axis to the target's LOS compensates for them. The sensors respond to angular accelerations, then, not rates. Since the acceleration for the examples given are very low, T would be greatly increased. This, in turn, would bring ω_v below the frequencies figured previously. Since Equations (9a) and (16a) are valid for $T \quad \omega_v^{-1}$, vibrations with frequencies from 0 to ω_v are used to compute A_N and A_p .

Vibration rate in the LOS perpendicular direction also causes image smear. Analysis in the preceding section is valid here alos. The equivalent of Equation (11) is

$$\dot{A}_p = \frac{\sigma_{LT} R_n}{t_i F} \tag{18}$$

where

$\dot{A}_p$ = maximum allowable linear vibration rate along the LOS perpendicular

LOS. The amplitude of linear motion in the LOS direction has a slight magnification effect on the target (see Fig. 17). The area which the target's image covers in the focal plane is expanded according to the ratio

$$\frac{R \pm A_L}{R} = \frac{a_2}{a_1} = \frac{a_1 \pm \Delta a_1}{a_1} \tag{19}$$

where

a_1 = area of image at time T_0

a_1 = a_2 a_1

a_2 = area of image at time T_1

a_L = amplitude of the vibration (-) sign means that A_L is towards the target / (+) sign means that A_L is away from the target

Equation (18) can be written

$$\frac{A_L}{R} = \frac{\Delta a_1}{a_1} \quad , \quad \Delta a_1 = \frac{A_L}{R} \; a_1 \tag{20}$$

Since Δa causes no change in the LOS, vibrations in the direction of LOS do not affect θ_{LOS} or range measurement.

The image is smeared over an area according to

$$a_1 = \frac{\Delta A_L}{R} \; a_1 \tag{21}$$

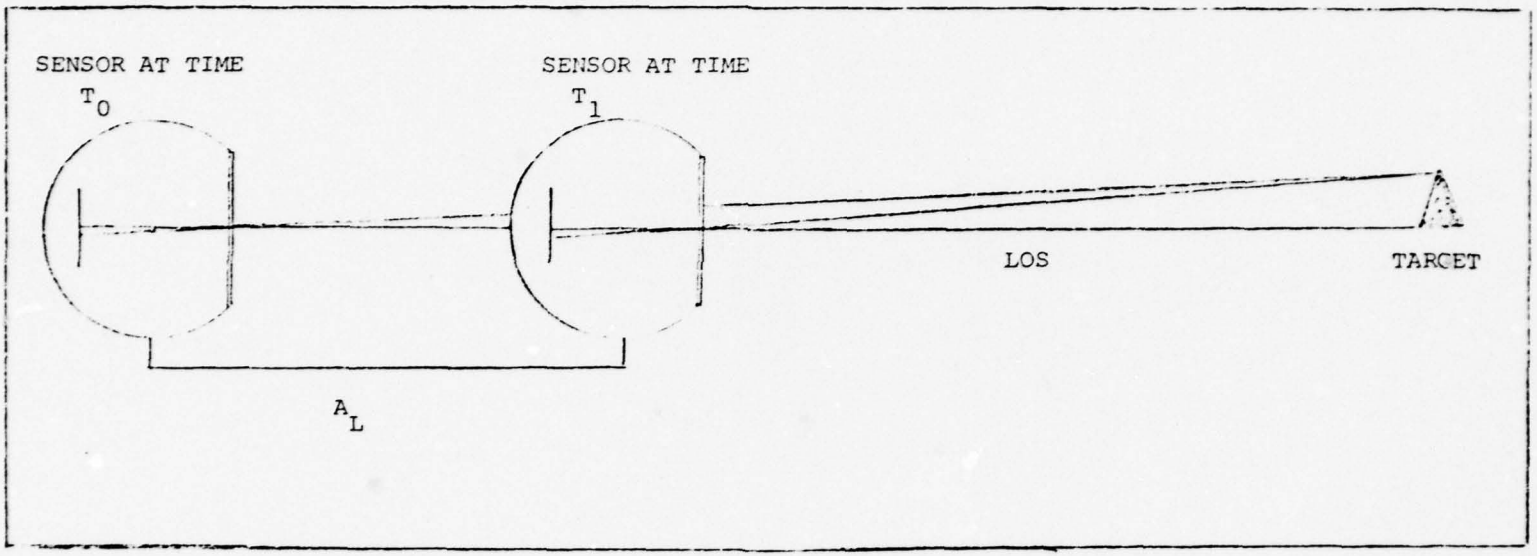

FIGURE 17. Linear LOS Vibration

where

$$\Delta A_L = \dot{A}_L t_i$$

and

$\dot{A}_L$ = rate of LOS vibration

t_i = integration period

When Δa is large enough, it affects correlation in the same manner as image smear did in the other directions. Since the image is expanding in both directions at once, the threshold value is expressed as an area. The equation for maximum vibration rate takes the form

$$\dot{A}_L = \frac{\sigma}{a} \frac{R}{t_i} \tag{22}$$

where

σ_a = threshold area referenced to a

a = area of the image a equilibrium

Angular Vibration Effects

Angular vibrations are handled in the same format as the linear vibrations. Their amplitude and rates about each of the three axes are analyzed with respect to sensor performance.

Angular Vibration About Sensor-Target Normal. Angular vibrations about the sensor-target normal are v_1 . The amplitude of these vibrations directly affects the measurement of azimuth and range (see Fig. 18). This angle is in the same plane as ϕ_a of Equation (11).

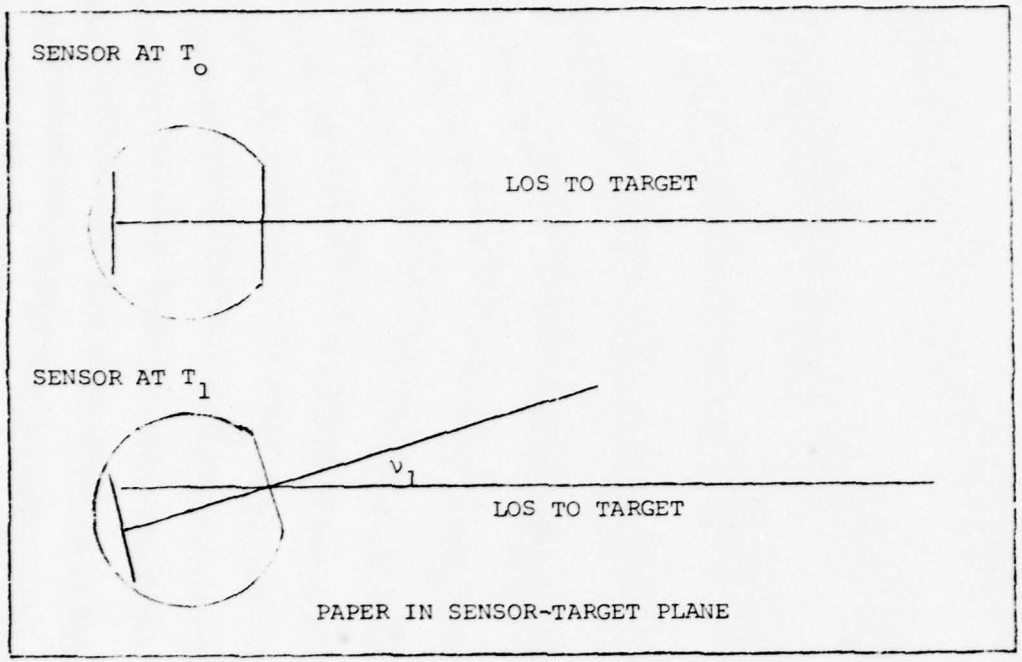

FIGURE 18. Angular Vibration About the Sensor-Target Normal

The difference here is that there is no dependence on range to the target. Analysis of the motion's effect on the stereometric system is exactly the same as for ϕ_a at frequencies above ω_v. Signal averaging as in Equation (14) does not average out ν_1 at frequencies below ω_v. Error in measuring α is equal to the sum of the squares of the amplitude of vibration for both sensors. Putting this in the form of an equation (see Fig. 14)

$$\Delta\alpha = \sqrt{2}\,\nu_1 \tag{23}$$

where ν_1 was assumed to be the same for each sensor. ν_1 calculated from Equation (21) is maximum allowable amplitude for angular vibrations.

The rate of these angular vibrations multiplied by the integration period and focal length gives the length of image smear in the LOS perpendicular direction. This can be compared to the threshold value for acceptable pointing accuracy. Solving the equation for angular rate gives the following equation.

$$\dot{\nu}_1 = \frac{\sigma_{LT}}{F\,t_i} \tag{24}$$

where

$\dot{\nu}_1$ = maximum allowable vibration rate.

Angular Vibration About LOS Perpendicular. Angular vibrations about the LOS perpendicular are ν_2. Amplitude of these vibrations has an effect on the elevation measurements by the sensors. When these vibrations have a frequency greater than ω_v, the vibration amplitude

can be averaged out. At ω_v and below, this vibrational amplitude will be measured as pitch variation. The desired pitch angle accuracy, $\Delta\theta_p$, is set equal to ν_2. In the form of an equation, the last sentence is

$$\Delta\theta_p = \nu_2 \tag{25}$$

Equation (12a) can be used to calculate the maximum ν_2 allowable to produce acceptable pitch information.

Rate of the angular vibration times the integration period times the focal length gives image smear in the sensor-target normal direction. As in the previous case, the threshold value for acceptable image smear, σ_{LT} will give maximum allowable angular vibration rate by

$$\dot{\nu}_2 = \frac{\sigma_{LT}}{t_i F} \tag{26}$$

where

$\dot{\nu}_2$ = maximum allowable vibration rate.

Angular Vibration About LOS. Angular vibrations about the LOS are ν_3. Amplitude of these vibrations have no direct effect on the pointing accuracy of the sensor. Angular rate can cause image smear if the amplitude of the vibration is large enough.

When the tracking sensor is working properly, the target's image is centered on the optical axis of the sensor. LOS and optical axis

are superimposed. Angular vibrations about this axis will make the target's image appear to rotate (see Fig. 19).

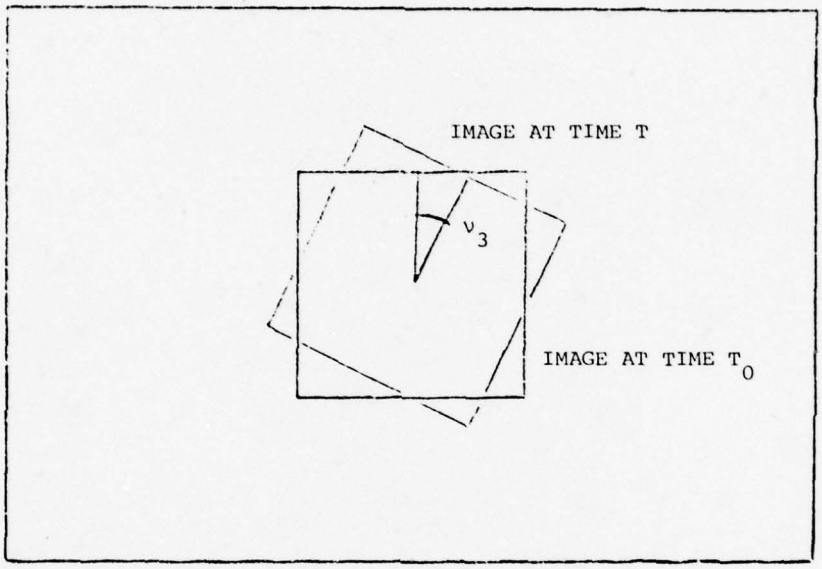

Figure 19. Image Rotation

Analysis of the effect of this kind of rotational smear on targets of various shapes can be done experimentally. The experiment should determine the amount of image rotation allowable before correlation processing is seriously degraded. If this value is designated as σ_{LOS}, then

$$\dot{\nu}_3 = \frac{\sigma_{LOS}}{t_i} \tag{27}$$

where

σ_{LOS} = threshold angle at which correlation processing is degraded

$\dot{\nu}_3$ = maximum allowable angular rate of vibration about LOS axis

This concludes the analysis of vibrations. Flexures are analyzed in the next section.

Flexures

Flexures are the same movements as vibration, only at a lower frequency. For this system, vibrations were considered low frequency at ω_v or less. Flexures fall into this category; therefore, they have already been analyzed in the vibration section.

Summary

This section analyzed the effects of vibrations and flexures on sensor performance. The goal of this analysis was to find parametric expressions for the effect of these vibrations and flexures. A coordinate system was established. Linear and angular vibrations were distinguished from each other.

Vibrations were analyzed first. Linear vibrations along the *sensor-target normal* affected elevation tracking performance. Averaging the sensor data will eliminate vibrations at frequencies greater than ω_v. Limiting amplitude for vibrations below ω_v and flexures is given by Equation (10).

$$A_n = R_n [\Delta\theta_p] \tag{10}$$

The limiting rate is calculated from Equation (11).

$$\dot{A}_n = \frac{\sigma_{LT} R_n}{t_i F} \tag{11}$$

Linear vibrations along the LOS perpendicular affect azimuth and range measurements. Averaging sensor data will eliminate vibrations above $_v$. For vibrations below $_v$ and flexures,

$$A_p = R_n \Delta\theta_a \quad \text{, for azimuth} \tag{12a}$$

$$A_p = \frac{B}{\sqrt{2}} \left(\frac{\Delta R}{R}\right) \quad \text{, for range} \tag{17}$$

Vibration rate is set by Equation (18).

$$A_p = \frac{\sigma_{LT} R_n}{t_i F} \tag{18}$$

Linear vibrations along the LOS have a slight magnifying effect. The rate of vibration is limited by Equation (21).

$$\dot{A}_L = \frac{\sigma_a}{a} \frac{R_n}{t_i} \tag{22}$$

Angular vibrations about the sensor-target normal affect ranging. Averaging sensor data will eliminate vibrations above ω_v . Vibrations below ω_v are flexures are limited in amplitude by

$$v_1 = \frac{\Delta\alpha}{\sqrt{2}} \tag{23}$$

Maximum angular rate is given by

$$\dot{\nu}_1 = \frac{\sigma_{LT}}{F\, t_i} \tag{24}$$

Angular vibrations about the LOS perpendicular affect elevation. Amplitude for vibrations below ω_v and for flexures is given by Equation (24). Maximum angle rate is given by Equation (25).

$$\nu_2 = \Delta\theta_p \tag{25}$$

$$\dot{\nu}_2 = \frac{\sigma_{LT}}{F\, t_i} \tag{26}$$

Angular vibrations about the LOS direction do not affect range or elevation tracking directly. They can cause image smear. Equation (26) gives the maximum angular rate for vibrations or flexures.

$$\dot{\nu}_3 = \frac{\sigma_{LOS}}{t_i} \tag{27}$$

Since the main distinction between flexures and vibrations is frequency, the equations derived for vibrations are valid for flexure.

In the next section, these equations will be used to aid in the placement of sensors on a tactical aircraft.

VII. Analysis Applied to F-15 Data

Introduction

This section takes the analytical expressions of Section VI and uses them to determine optimum sensor placement. The equations in Section VI determine maximum allowable vibration amplitudes and rates. Expressions in this section determine vibration amplitude and rate of the sensor as a function of position when possible. Therefore, it is possible to find a position of the sensor such that amplitudes and rates are less than the maximum allowable.

The leading edges of the wings are the primary candidates for location of the sensors. The twin tail structure of the F-15 is also considered. An exact relationship between vibrations and position along the leading edge of the wing would require analysis by means of finite elements. Analysis of this type had not been accomplished on a fighter aircraft previously, and such an analysis is not within the scope of this thesis.

Some flight test data is available for F-15 wing and tail structures. The flight tests were conducted to determine the maximum vibrational environments at certain positions on the wing. The data collected on these flight tests is in the form of power spectral density, PSD (Figs. 20, 21, 22). In order to find the mean value for amplitude and rate of the vibrations, it is necessary to use the relationships derived in Appendix A:

$$\bar{V}(t) = \left[\int_0^\infty d\omega \, \frac{\rho_a(\omega)}{\omega^2}\right]^{\frac{1}{2}} \quad [G] \tag{27a}$$

$$\bar{X}(t) = \frac{1}{2}\left[\int_0^\infty d\omega \, \frac{\rho_a(\omega)}{\omega^4}\right]^{\frac{1}{2}} \quad [G] \tag{27b}$$

where

$\bar{V}(t)$ = average velocity of the vibrating sensor

$\bar{X}(t)$ = average displacement of the vibrating sensor

$\rho_a(\omega)$ = power spectral density

G = earth's gravitational acceleration constant at sea level

The factor of G is required because the data was originally recorded in G's squared.

All the data available is from linear accelerometers. Angular vibration data is not available because adequate angular accelerometers are not available (Ref. 17).

Data collected for the F-15 wing and tail represent severe vibrational environments. Data representing normal flight conditions is better suited to this analysis. However, such data is not available at this time. The rates and amplitudes computed from the available data should be considered as maximum values and not the normal values. Two types of maneuvers were performed to generate the vibrations. They were a windup turn and a symmetric pullup. Of these maneuvers, the windup turn induces the greatest vibrations. When possible then, the data for the symmetrical pullup maneuver will be used in preference to the windup turn data.

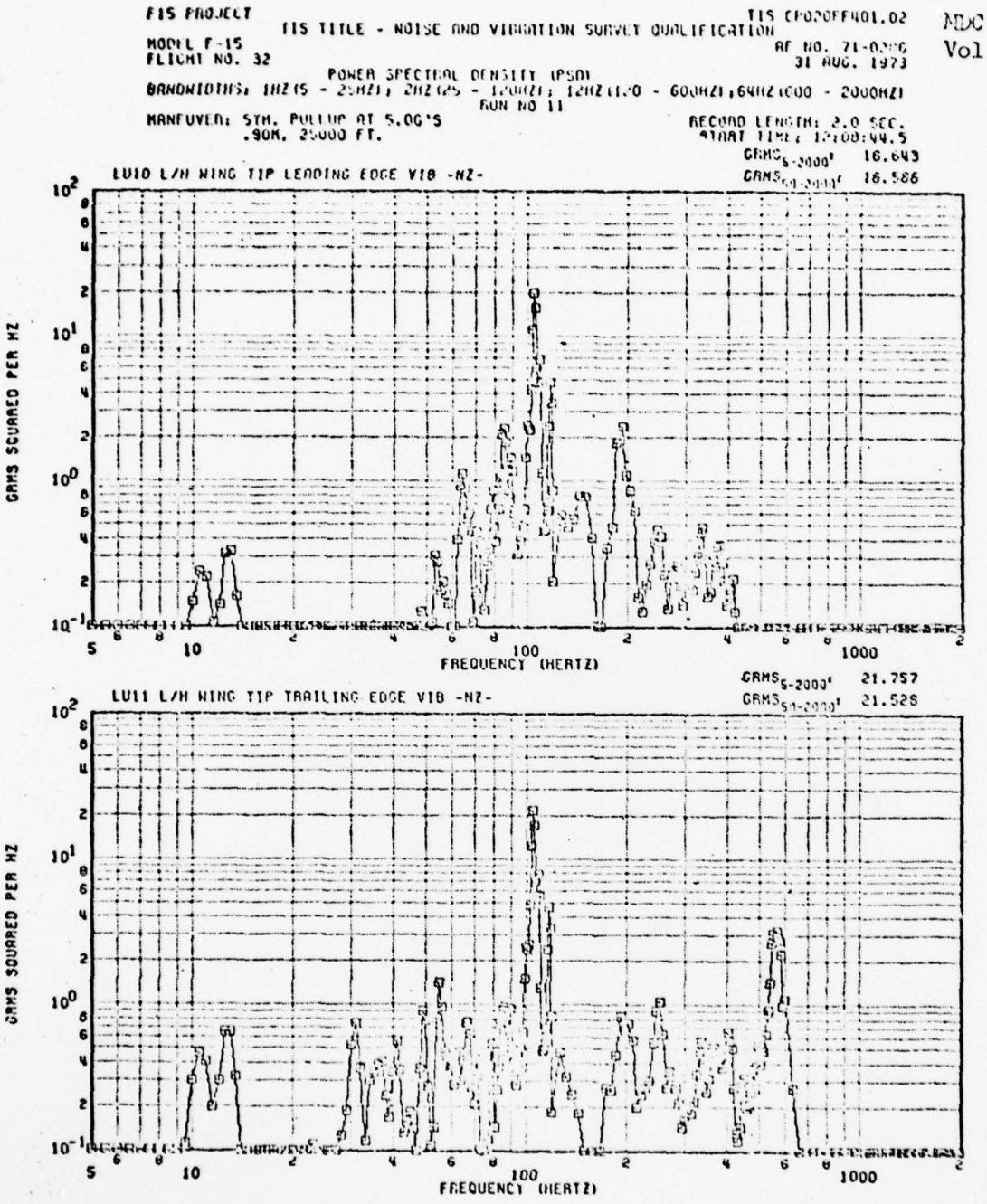

FIGURE 20 Power Spectral Density for LU10

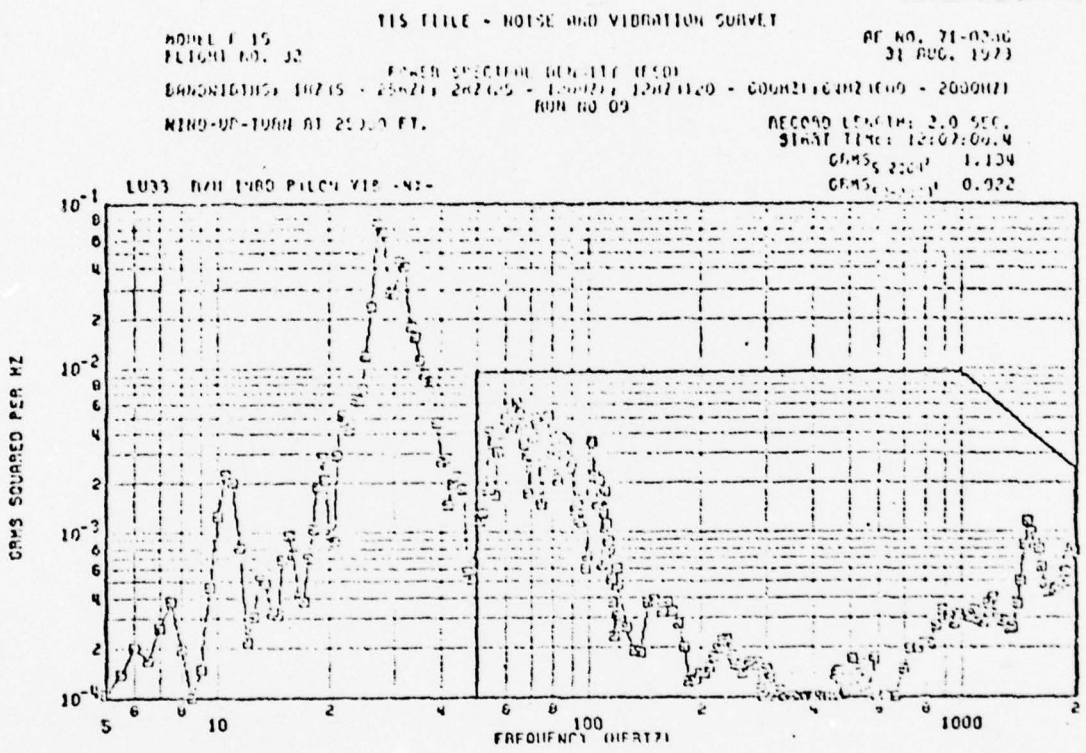

FIGURE 21 Power Spectral Density for LU33

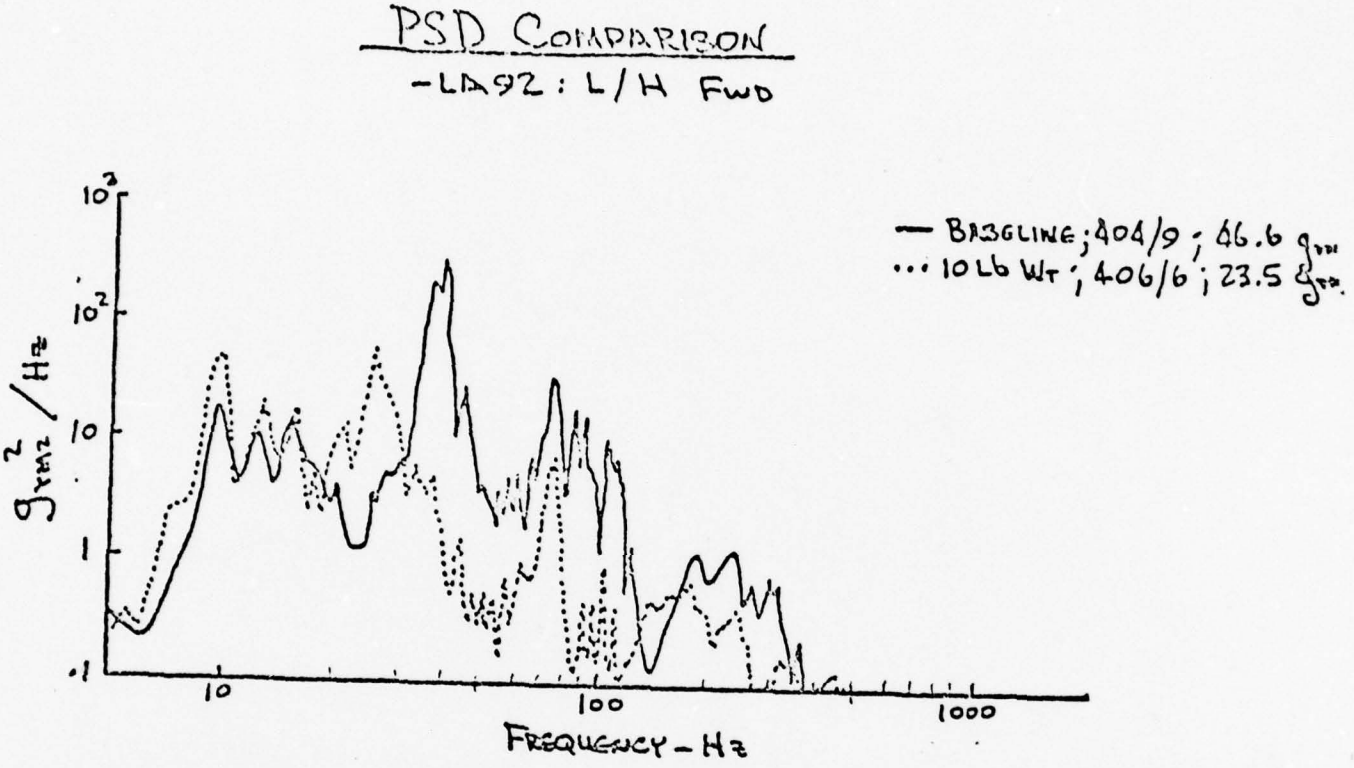

FIGURE 22 Power Spectral Density for Tail

The limit of integration for Equations (27a) and (27b) represent the entire spectrum of frequencies. The data, however, is limited to a minimum of 5 Hz because the accelerometers used to measure vibrational accelerations had a minimum frequency range of 5 Hz. However, it is likely that there are no vibrational modes of the wing or tail below 5 Hz.

If the wing is modeled as a tapered cantilevered beam, the frequency of the first mode of vibration is given by (Ref. 16:456-470)

$$f = \left(\frac{5.315}{2\pi}\right) \frac{b}{l} \left(\frac{E}{3\rho}\right)^{\frac{1}{2}}$$

where

b = width of the beam at the support

l = length of the beam

E = modulus of elasticity of aluminum

ρ = density of the beam density of aluminum

Density of the beam is assumed to be approximately one-tenth of the density of solid aluminum. Width of the wing at the wing root is approximately 8 inches when viewing the wing head-on. Width of the wing at the root is 225 inches when viewing the wing in planform as in Figure 23.

Width of the tail at the fuselage is 6.5 inches when viewed head-on. The wing is 256 inches long from fuselage to wing tip. The tail is 124 inches high from the fuselage. Using these figures, the frequencies of the first mode of vibration are

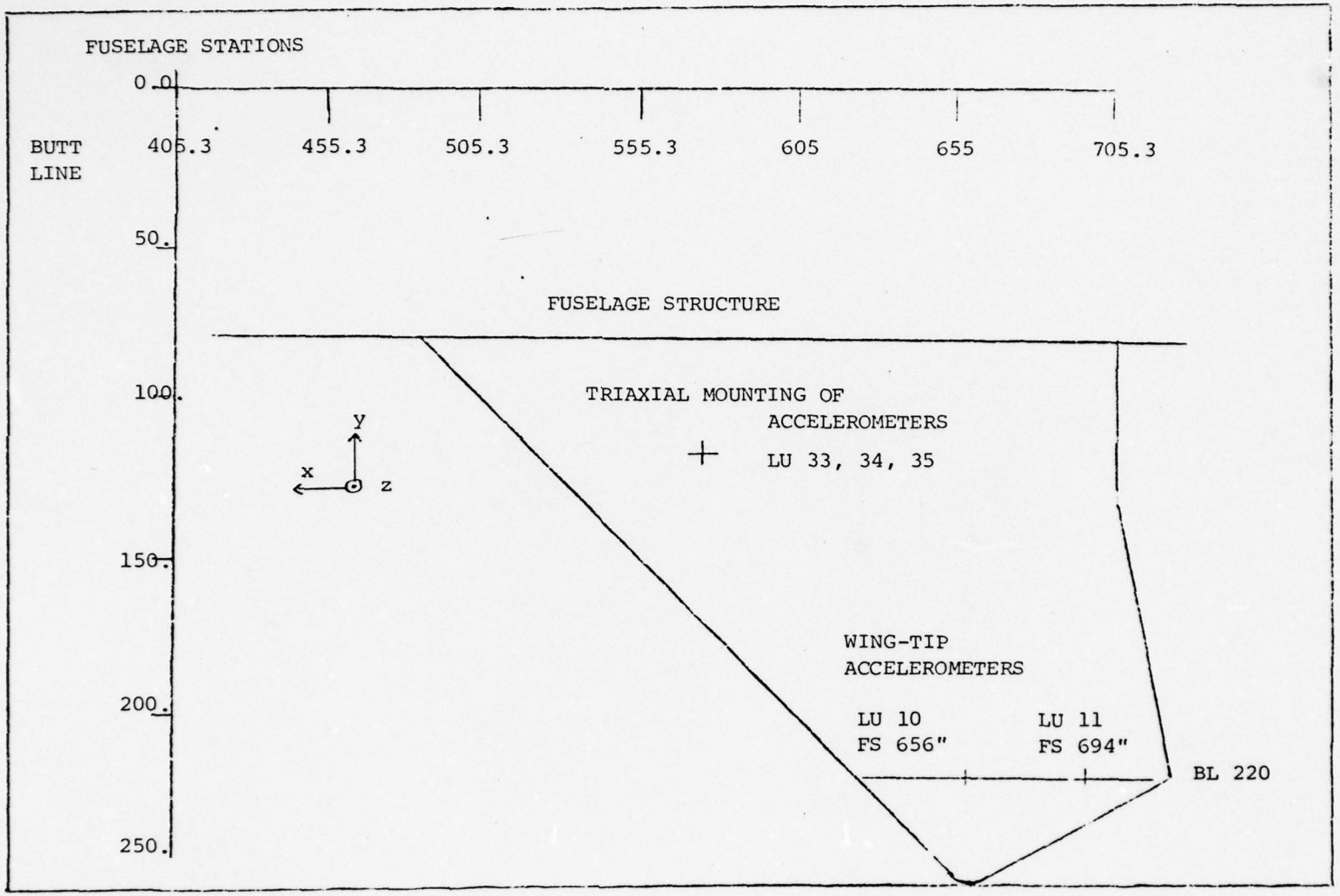

FIGURE 23. F-15 Wing Top Planform View

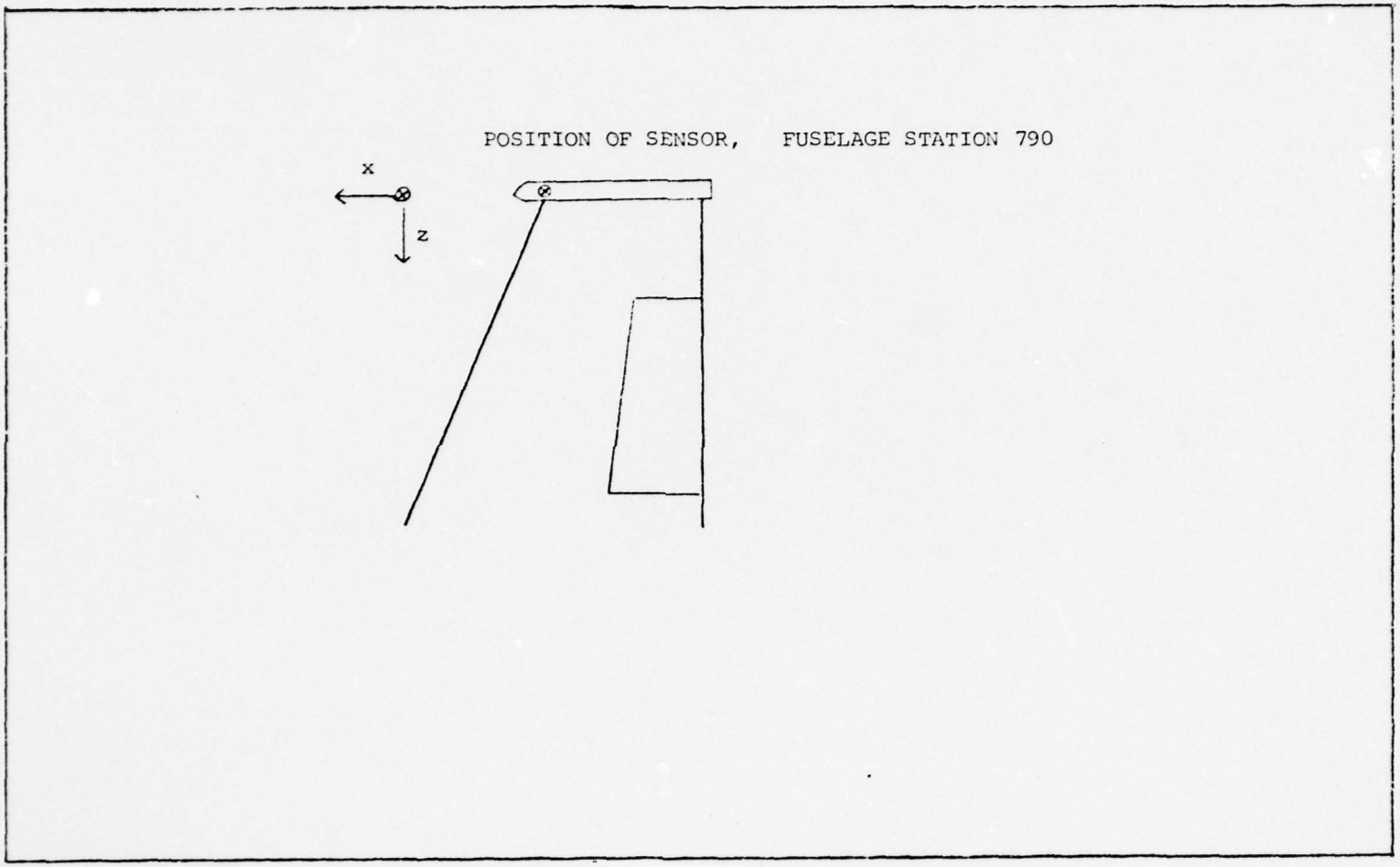

FIGURE 24. Profile of F-15 Tail

$$f_{\text{wing z}} \simeq 5 \text{ Hz}$$

$$f_{\text{wing x}} \simeq 150 \text{ Hz}$$

$$f_{\text{tail y}} \simeq 18 \text{ Hz}$$

where

$f_{\text{wing z}}$ = frequency of wing vibrations in the z direction

$f_{\text{wing x}}$ = frequency of wing vibrations in the x direction

$f_{\text{tail y}}$ = frequency of tail vibrations in the y direction

The frequency computed for the first mode of wing vibration in the x direction is obviously too high. This is due to the inaccuracy of the model used for wing vibrations in this direction. $f_{\text{tail y}}$ also seems high. However, $f_{\text{wing x}}$ and $f_{\text{tail y}}$ are certainly greater than $f_{\text{wing z}}$. The cantilevered beam model for the wing vibrating in the z direction is probably a good approximation because b is so much smaller than l. The estimations on ρ and E will not change $f_{\text{wing z}}$ more than an order of magnitude. For the purpose of this analysis, then, the minimum frequency for wing or tail vibrations in any of the directions considered is 5 Hz.

The upper limit on frequency of vibration is ω_v. In Section VI, ω_v is shown to have a range of values, depending on T. T, in turn, depended on the type of target and attack. From Figures 14c, 15b, and 16a, T is an interval of time between 4 seconds and .021 seconds. In computing $\bar{X}$ and $\bar{V}$ from the data, ω_v = 95 Hz gives the largest values, while ω_v = .25 Hz yields the least. Since the frequency of the first vibration mode of any of the structures is 5 Hz, an

ω_v below that frequency yields $\bar{X}$ and $\bar{V}$ of 0 . The two extremes for $_v$ make analysis of the data somewhat uncertain. A more reasonable cut-off for $_v$ is 10 Hz. This frequency represents a period, T , of .2 seconds which is possible for most parts of the missions discussed in Section VI.

Table V is a list of the values for $\bar{X}$ and $\bar{V}$ calculated at positions LU 10 , LU 11 , LU 33 and the tail. See Figures 23 and 24 for these locations on the aircraft. The accelerometers at positions LU 10 and LU 11 measured acceleration in the z direction (Fig. 23). The accelerometer at position LU 33 measured accelerations in the x direction and the tail accelerometer measured accelerations in the y direction. $\bar{X}$ and $\bar{V}$ were computed using symmetric pullup data at positions LU 10 and LU 11 , while windup turn data were used at the other two locations.

If the values for $\bar{X}$ and $\bar{V}$ at ω_v = .25 Hz are designated as a , and at ω_v = 10 Hz as m , and at 95 Hz as b , then the mean value for these quantities, $\bar{u}$, is estimated by

$$\bar{u} = \frac{a + 4m + b}{6}$$

with a variation, σ^2 , estimated by

$$\sigma^2 = \left(\frac{b - a}{6}\right)^2$$

The values listed under $\bar{u}$ will be used to determine the placement of the sensors.

TABLE V. Analysis of PDS

($\bar{V}$ in ft/sec, $\bar{X}$ in inches)

POSITION	ω_v 95 Hz $\bar{V}/\bar{X}$	ω_v 10 Hz $\bar{V}/\bar{X}$	ω_v .25 Hz $\bar{V}/\bar{X}$	$\bar{u}$	σ^2
LU 10	7.0 4.1	3.5 3.8	0 0	3.5 3.2	1.2 .7
LU 11	7.3 4.2	3.5 3.8	0 0	3.5 3.2	1.2 .7
LU 33	.67 .24	.15 .13	0 0	.21 .13	.11 .04
Tail	52 19	28 18	0 0	27 15	8.7 3.2

In analyzing the effects of vibrations on the sensors, it is convenient to clearly describe θ_p and θ_a. These angles are depicted in Figure 25. Azimuth, θ_a, is measured in the x-y plant using a line in the x-y plane perpendicular to the azimuth line and through the origin.

The following subsections use the flight test data and equations from Section VI to determine suitable placement of the electro-optic sensors. Analysis will start with the twin tails.

Tail Vibrations

Sensors located at the position of accelerometer in Figure 24 undergo linear vibrations of 15 inches in the y direction. Assuming both tail structures behave the same, each sensor will undergo displacements of (15 inches) $\cos \theta_A = A_p$.

Equation (17) gives the relationship

$$\frac{A_p}{R_n} = \Delta\theta_a$$

where $\Delta\theta_a = \Delta\theta_{LOS}$ is given as 1 mrad in Table III. If A_p = 15 inches, then R_n = 1250 ft. This, then, is the minimum range of the stereometric tracker mounted on the tail.

The direction of the amplitudes of these vibrations is along y, which is also the direction of the base line. Therefore, $A_p = \Delta B$. If the errors in range due to α and F are ignored, then

$$\frac{\Delta R}{R} = \frac{\Delta B}{B} = \frac{A_p}{B} \qquad (28)$$

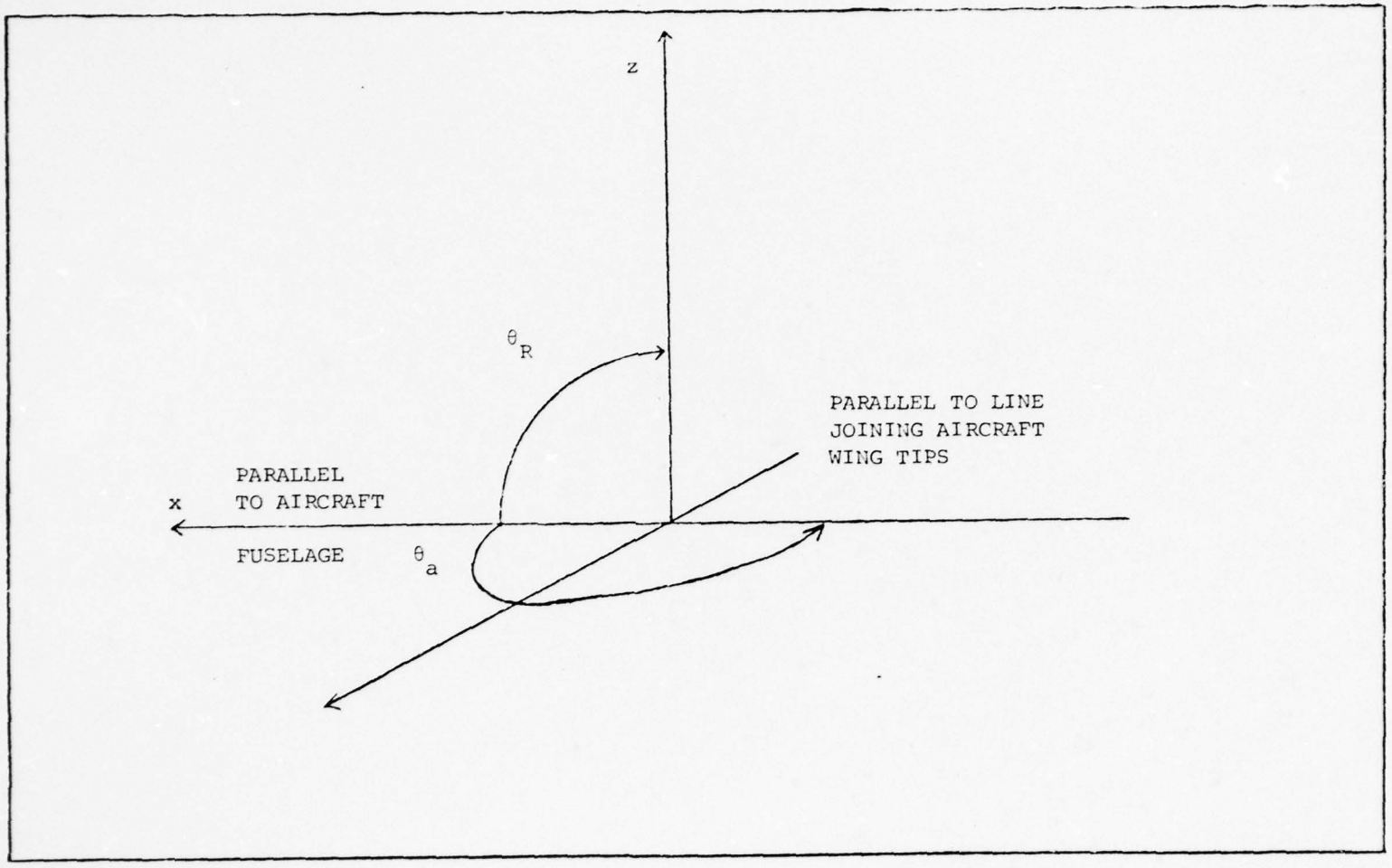

FIGURE 25. Aircraft Coordinate System

From Table III, $R = 1.1$ NM when $R = 89$ NM . Solving Equation (28) for A_p gives $A_p = 6$ inches if $B = 40$ ft.

If σ_{LT} is equal to the horizontal dimension of one pixel, the maximum allowable rate of vibration is

$$\dot{A}_p = \frac{\sigma_{LT} R_n}{t_i F} \quad .41 \text{ ft/sec} \tag{18}$$

Image smear, then, will cause the greatest problem. In view of the 27 ft/sec rate from the data for the tail pods, they seem to be an unsuitable place for the sensors.

Wing Vibrations

A search of F-15, F-16 and A-10 flight test data produced limited data for linear vibrations of the F-15 wing. RMS amplitudes and rates of vibration are given in Table V. Linear vibration data is recorded in the x and z direction.

In order to have a relationship between vibrational amplitude and position along the leading edge of the wing, it was necessary to model the wing as a cantilevered beam of variable cross section (Ref 16:465-470). The details of the analysis can be found in Appendix B. By means of this analysis, the first mode of vibration is approximated by

$$y_1 = a_1 \left(1 - \frac{d}{\ell}\right)^2 \tag{29}$$

where

d = distance from wing tip to position of interest

l = length of the wing

AD-A064 688 AIR FORCE INST OF TECH WRIGHT-PATTERSON AFB OHIO SCH--ETC F/G 17/8
PARAMETRIC ANALYSIS OF STEREOMETRIC TRACKER FOR USE IN TACTICAL--ETC(U)
OCT 78 K F SCHROEDER

UNCLASSIFIED AFIT/GEP/PH/78D-11 NL

2 OF 2
AD
A064688

END
DATE
FILMED
4-79
DDC

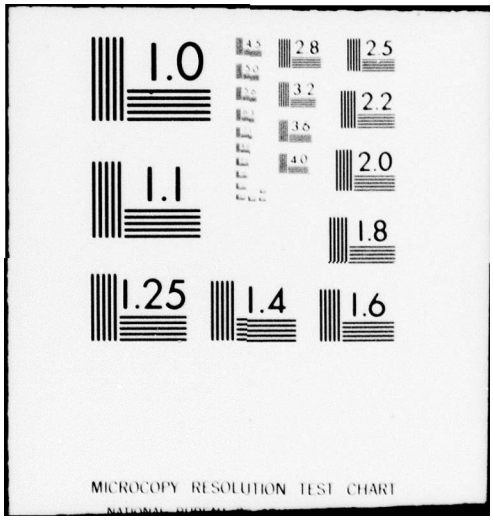
1.0
1.1
1.25
1.4
1.6
1.8
2.0
2.2
2.5
2.8
3.2
3.6
4.0
MICROCOPY RESOLUTION TEST CHART

a_1 = amplitude coefficient

y_1 = perpendicular amplitude of the beam

The results of this analysis must be used with caution. The model falls short of the wing in a number of ways. First, the wing vibrates in three dimensions, not just two independent planes. The wing was modeled as a symmetric wedge. In reality, it is a complex form with little symmetry in the $x - y$ plane. As can be seen from the PSD charts, there are many vibrational frequencies. RMS vibration amplitude is computed from the data and taken as the amplitude of only the first mode of the bending beam. This will give too large an amplitude for the first mode. The model is justified because it is the best available to determine a relationship between d and y_1 given the lack of available data for the wings. With these things in mind, linear and angular vibrations will be analyzed.

The wing will be analyzed at position LU 10 first. Linear vibrations below ω_v in the z direction cause errors in measuring the elevation angle. From Table III, the accuracy desired is .1 mrad. A_N = 3.2 inches from Table V. Using Equation (10),

$$R_n = \frac{A_N}{[\Delta\theta_p]} = 2.66 \text{ ft}$$

A_N can be increased 6 inches if an R_n = 500 ft is desired.

Using Equation (29) where it is understood that y_1 is in the z direction, a_1 can be found by letting $y_1 = A_N$ and d = the position of LU 10 . z_a is the amplitude of the vibration.

$$a_1 = \frac{y_1}{(1 - d/\ell)^2} = 4.6 \text{ inches} \qquad (29a)$$

If Equation (29) is solved for d and if y_1 is set equal to the desired amplitude of vibration, d will represent the minimum distance from the wing tip. Thus, Equation (29) becomes

$$d = \ell \left(1 - \left|\sqrt{\frac{y_1}{a_1}}\right|\right) \qquad (30)$$

If $y_1 = A_n$, then $d = 29$ inches, which is 147 inches from the fuselage. Since the fuselage is 160 inches wide, $B \simeq 38$ ft.

If $_{LT}$ is equal to the vertical dimension of one pixel, the maximum vibration rate will be

$$\dot{A}_N = \frac{\sigma_{LT}}{t_i} = .67 \text{ ft/sec} \qquad (11)$$

where

$\dot{A}_N = \bar{\dot{Z}} \cos \theta_p$

$\bar{\dot{Z}}$ = mean of the vibrations in the z direction

Again, this is a severe restriction since $\bar{\dot{Z}}$ was 3.5 ft/sec.

Unfortunately, no equations like (29) or (30) exist for vibrational rates. If they did, it would be possible to determine d such that the vibration rate in the z direction is acceptable.

Vibrations in the z direction will give rise to $\dot{A}_L$ as the sensor follows a target in elevation.

$$A_L = A_a (\sin \theta_p) \quad (\cos \theta_a) \tag{31}$$

When the sensor is looking directly up or down, $\theta_p = 90°$, $\theta_a = 0$, and $A_L = Z_a$. Vibration in this direction has no effect on tracker performance.

The other direction of linear wing vibration is in the x direction. Vibration in the x direction is measured by the accelerometer at LU 33 . Using the RMS value of x_a , amplitude of the vibration in the x direction, as y_1 , $a_1 = 3.3$ inches by Equation (29).

The amplitudes and rates of wing vibrations are related to sensor vibrations by

$$A_N = \bar{X}_a \sin \theta_p \quad , \quad \dot{A}_N = \dot{\bar{X}}_a \sin \theta_p \tag{32}$$

$$A_p = \bar{X}_a \sin \theta_a \quad , \quad \dot{A}_p = \dot{\bar{X}}_a \sin \theta_a \tag{33}$$

$$A_L = \bar{X}_a \cos \theta_p \cos \theta_a \quad , \quad \dot{A}_L = \dot{\bar{X}}_a \cos \theta_p \cos \theta_a \tag{34}$$

where

$\dot{\bar{X}}_a$ = rate of vibration in the x direction

The requirements on the amplitudes of sensor vibration remain the same; it is only the direction of vibration which has changed. Thus, the requirements $A_n = 6$ inches , $\dot{A}_n = .67$ ft/sec , and $\dot{A}_p = .41$ ft/sec remain unchanged. For a baseline of 40 ft, $A_p = 5.9$ inches .

From Table V, $\bar{X}_a = .13$ inches . The location of the accelerometer

which produced this data was 115 inches from the aircraft centerline. If a baseline of 40 ft is desired, the mean amplitude of the vibration at the new position can be computed using Equation (29a). First, solving for a_1 at LU 33 ($d = 141$ inches, $y_1 = \bar{X}_a$)

$$a_1 = \frac{\bar{X}_a}{(1 - d/1)^2} = 3.14 \text{ inches}$$

If the two electro-optic sensors are placed 40 ft apart, the mean value of $\bar{X}_a$ will be increased to

$$\bar{X}_a = a_1(1 - d/1)^2 = 2.6 \text{ inches}$$

Structural vibrations of this amplitude are within the limit set by A_p and A_n.

There are no angular vibration data for the wing. Equation (29) can be used to transform the linear data to angular data in the following manner:

since

$$y_1 = f(d)$$

where y_1 and d are orthogonal

$$\theta = \frac{d}{d(d)} y_1 = \frac{d}{d(d)} f(d)$$

$$= \frac{-2 a_1}{\ell} \quad (1 = \frac{d}{\ell}) \qquad (35)$$

where

θ = angle of the tangent at the point d measured in radians

For example, the angular deflection at d = LU 10 , in the y - z plane, is $\bar{\theta}_2 = .13$ rad = 7.25° .

Amplitudes and rates of wing angular vibrations are related to sensor angular vibrations by

$$\nu_1 = \bar{\theta}_z \sin \theta_p \cos \theta_a \quad , \quad \dot{\nu}_1 = \dot{\bar{\theta}}_z \sin \theta_p \cos \dot{\theta}_a \tag{36}$$

$$\nu_2 = \bar{\theta}_z \sin \theta_a \cos \theta_p \quad , \quad \dot{\nu}_2 = \dot{\bar{\theta}}_z \sin \theta_a \cos \dot{\theta}_p \tag{37}$$

$$\nu_3 = \bar{\theta}_z \cos \theta_p \cos \theta_a \quad , \quad \dot{\nu}_3 = \dot{\bar{\theta}}_z \cos \theta_p \cos \theta_a \tag{38}$$

From Section VI, angular vibrations with frequencies below ω_v have a maximum amplitude of $\nu_1 = \frac{\Delta\alpha}{\sqrt{2}}$ (Eq. (23)), $\nu_1 = 5.6 \times 10^{-5}$ rad , and for $\nu_2 = \Delta\theta_p$ (Eq. (25)), $\nu_2 = .1$ mrad . The angular rates of these vibrations are $\dot{\nu}_1 = \frac{\sigma_{LT}}{F\, t_i}$ (Eq. (24)), $\dot{\nu}_1 = 2.47 \times 10^{-4}$ rad/sec , $\dot{\nu}_2 = \frac{\sigma_{LT}}{F\, t_i}$ (Eq. (26)), $\dot{\nu}_2 = 4.12 \times 10^{-4}$ rad/sec, $\dot{\nu}_3 = \frac{\sigma_{LT}}{t_i}$ (Eq. (27)), $\dot{\nu}_3 = 9.07$ rad/sec .

If the electro-optic sensors have a baseline of 40 ft, $\bar{\theta}_z = 4.7 \times 10^{-2}$ rad . By Equation (36) , $\bar{\theta}_z \sin \theta_p = \nu_1$ when the target is directly in front of the fighter. Since $\bar{\theta}_z = 4.7 \times 10^{-2}$ and $\nu_1 = 5.6 \times 10^{-5}$ rad , an elevation angle of $\theta_p = \text{arc sin } \nu_1/\bar{\theta}_z = 1.2 \times 10^{-3}$ rad is the maximum allowable before $\bar{\theta}_z$ begins to influence the range accuracy of the tracker. If θ_p were as high as 30° , the position of the sensors would have to be adjusted so that $\bar{\theta}_z = 2\nu_1$.

From Equation (35) and $\bar{\theta}_z = 2_1$:

$$d = \frac{\ell^2(2\nu_1)}{2a_1} - \ell = -176 \text{ inches} \tag{39}$$

The minus sign has no significance here. In order to meet the requirement of ν_1 , the sensor must be placed next to the fuselage.

Since the cantilevered beam model does not transform angular rates, there are no comparisons to make.

For wing vibrations in the x - y plane, $\theta_x = 7.6 \times 10^{-3} = .43°$ using Equation (35) and d = LU 33 . θ_x is related to the sensor amplitudes by

$$\nu_1 = \theta_x \cos \theta_p \tag{40}$$

$$\nu_3 = \theta_x \sin \theta_p \tag{41}$$

As in the case for θ_z , θ_x can be equal to ν_1 or ν_3 given the proper azimuth or elevation angle. Even though $\theta_x < \theta_z$, it still is not small enough to meet the restriction of ν_1 . Using Equation (39), d ≈ 176 inches , which is next to the fuselage. However, θ_z is more restrictive, so that the value of d it predicts must be honored.

Summary

This section used the equations in Section VI and data from flight tests to determine optimum positions for the optical trackers. The data available was in the form of linear PSD. A simplified program calculated

RMS amplitudes and rates from the data. It was necessary to model the wing as a cantilevered beam in order to determine sensor placement.

Analysis of the tail data indicated that the amplitude of the linear vibrations is too large by a factor of 15:6 . The mean rate of vibration at the tail was also larger than that allowed for an image smear of one pixel. The tail is not a suitable location for the electro-optic sensors because of the vibration.

Wing vibrations were analyzed with the aid of Equation (30).

$$d = \ell \left(1 - \left| \sqrt{\frac{y_1}{a_1}} \right| \right) \tag{30}$$

The mean amplitude of linear vibration in either the $x - y$ or $y - z$ plane is small enough that it does not affect the tracker performance. The mean angular rate $\dot{\vec{z}}$ (LU 10) is an order of magnitude higher than $\dot{A}_n$.

Equation (39) was used to find an acceptable position in terms of angular vibration amplitude.

$$d = \frac{\ell^2 \theta}{2a_1} - \ell \tag{39}$$

v_1 was the most restrictive angular amplitude. It caused the sensors to be placed next to the aircraft fuselage.

It must be remembered that the flight conditions under which this data were taken are worst-case vibrational environments. Normal flight conditions would cause much less vibration. Also, the model used to determine placement of the sensors on the wing is severely limited in scope.

VIII. Conclusions and Recommendations

Summary

The objective of this thesis is a generalized parametric trade-off analysis of a passive stereometric tracker. The stereometric tracker uses two focal plane array sensors to track the target LOS. Azimuth and elevation are measured directly from the sensor's LOS. Range is computed from Equation (4), $R = B/\alpha$, where $\alpha = \theta_1 - \theta_2$.

Analysis of tracker performance centered on the system's angular resolution, baseline separation and the effects of aircraft vibrations and flexures on range finding accuracy. Performance criteria were specified in Section III and were transformed into sensor criteria in Section VI. The effects of aircraft vibrations and flexures on tracking performance were analyzed in Section VII and put into analytic expressions. Flight test data was used to find optimum placement of optical sensors on an F-15.

In Section IV, correlation between the sensors was found to be the most accurate means of determining α . Once the sensors are split, however, a means of maintaining optical alignment to 1 mrad is necessary. The means of measuring alignment to 1 mrad between two electro-optic sensors were not investigated.

Assuming that some means is found either to measure or maintain optical alignment between sensors, range tracking can be improved by increasing baseline separation (Ref. Equation (6)). Aircraft structures best suited are the wings and the twin tail design of some fighters. These structures are subject to severe vibrational and flexure environments.

Very little data are available on these structures to characterize their response to flight conditions. Information which is available is in the form of linear PSD. Angular vibration information is critical in evaluating the performance of an optical system. Some evaluation can be made using techniques described in References 17, 18, 19 and 20. However, as stressed in those references, these are not substitutes for direct measurement of angular vibration data.

By modeling the aircraft wing as a tapered, cantilevered beam, a trade-off between baseline separation and angular vibration can be made. Optimum position of the sensor using these two factors requires that the sensors be placed next to the fuselage. This is where $\Delta\alpha$ is as small as required for the desired range accuracy. However, this position is unsuitable due to the interference of the fuselage with the tracker's field of regard.

Conclusions

1. The means of maintaining or measuring alignment between remotely placed optical sensors is a major problem to be overcome.

2. A more accurate relationship between position and vibration at that position is required.

3. Angular vibration data is required to adequately analyze the system. Angular vibrations were much more detrimental to the tracker's performance than the linear vibrations.

4. Vibrations and flexures below ω_v drive the design of the system to a single unit with the optical sensors rigidly mounted.

5. The passive stereometric has the potential to give an aircraft the element of surprise when attacking a target. The element of surprise is particularly useful for tactical aircraft.

Recommendations

The following items should be considered before evaluting remotely placed sensors for stereometric tracking.

1. A means of measuring or maintaining optical alignment to 1 mrad should be investigated.

2. A finite element analysis should be made on the wing and tail structures to compute angular as well as linear vibration data.

3. A means of collecting angular vibrations of aircraft structures in flight should be found to validate recommendation 2.

4. The investigation into extending the range of a passive stereometric tracker should be continued because of its tactical advantages.

Bibliography

1. AF Contract F33615-78-C-1562, Advanced EO Tracker for Tactical Fighters. Wright-Patterson AFB:ASD/PMREB.

2. Morrison, P. and Walker, P.R., "A New Strategy for Military Spending," Scientific American, 239(4):48-61 (October 1978).

3. Stevens, R.R., Flight Dynamics Engineer, ASD/ENFY (telephone conversation). Wright-Patterson AFB, August 1978.

4. Hudson, R.D. and Hudson, J.W., "The Military Applications of Remote Sensing by Infrared," Proceedings of IEEE, 63(1):104-128 (January 1975).

5. Stein, K.J., "Pave Tack Pods Enhance Target Tracking Capacity," Aviation Week and Space Technology, 108:57 (February 1978).

6. Brownlow, C., "F-15, F-14 Show Foxbat Attack Capacity," Aviation Week and Space Technology, 99(7):16-17 (August 1973).

7. Pryor, Paul L., Sensor Performance and The Vehicle. Wright-Patterson AFB, Ohio:Air Force Avionics Laboratory, January 1970. (AD 751 969)

8. Proposal 3210-253, Advanced E-O Tracker for Gun Director System. Vol. I Phase I. Barrington, Illinois: CAI, Division of Bourns, Incorporated, 1977.

9. Burt, D.J., Coltman, H.D. and Simpson, P.I., "Charge-Coupled Devices," GEC Journal of Science & Technology, 41(2&3):53-62 1974.

10. Proposal 3210-253-3, Advanced E-O Tracker for Tactical Fighters. Barrington, Illinois: CAI, Division of Bourns, Incorporated, 1978.

11. Harris, R.A., Masters, R.M. and Wakefield, C.D., Co-ordinate System Alignment Technology Final Task Report. Cambridge, Massachusetts: The Charles Stark Draper Laboratory, Inc., 1976.

12. Shankland, D., Lecture on Signal Processing, School of Engineering, Air Force Institute of Technology, Wright-Patterson AFB, Ohio, 1978.

13. F/TF-15 Final Test Results Noise and Vibration Survey and Air-to-Air Missile Environment Survey (TIS Nos. CP 020FF401.01 and .02, CP 020FT401.01 and CP 020FF404.01) Vol II Book 1 Clean Airplane Measurands LA16 - LU16. Report MDC A3290. Flight test results in the form of graphs of PSD. St. Louis, Missouri: McDonnell Douglas Corporation, 1975.

14. ---Book 7 Pylon and Pylon Mounted Stores. Flight test results in the form of graphs of PSD. St. Louis, Missouri: McDonnell Douglas Corporation, 1975.

15. Frost, W., Graphs of PSD for the F-15 Tail Pods to be published in an ASD report. Title not yet determined.

16. Timoshenko, Stephen, Young, D.H. and Weaver, Jr. W., Vibration Problems in Engineering (Fourth Edition). New York: John Wiley & Sons, Inc., 1974.

17. Whaley, P. Wayne and Obal, Michael W., Angular Vibration Measurement Techniques. Wright-Patterson AFB: AF Flight Dynamics Laboratory.

18. ---Vibration Using Conventional Accelerometers. The Shock and Vibration Bulletin, Part 3 or 4 Parts. Washington, D.C.: Naval Research Laboratory, 1977.

19. Lee, J. and Whaley, P.W., "Prediction of the Angular Vibration of Aircraft Structures." Prescription of angular vibrations from linear vibrations. Journal of Sound and Vibration 49(4):541-549. Wright-Patterson AFB, Ohio: AF Flight Dynamics Laboratory, 1976.

20. Brown, D.L. and Whaley, P.W., Prediction of Angular Disturbances from Airframe Members to Airborne Electro-Optical Packages. Angular vibrations from linear vibrations. Wright-Patterson AFB, Ohio: Air Force Flight Dynamics Laboratory, 1977.

Appendix A

Integration of Power Spectral Density (Ref. 12)

Flight test data is collected in the form of acceleration history on tape. The acceleration data is transformed into power spectral density by

$$E\{a(t)\ a(t')\} = \phi(t - t') = \int d\omega\ e^{i\omega(t-t')} \rho_a(\omega)$$

where

$E\{\ \}$ = expectation value of the term in brackets

$\phi(\ )$ = autocorrelation of the function in time

ω = frequency

$t + t'$ = time

$\rho_a(\omega)$ = $2\pi\left|\bar{a}(\omega)^2\right|$ = energy density spectrum of $a_1(t)$ or power spectral density

and

$$a_1(t) = \frac{1}{\sqrt{2\pi}} \int_{-\infty}^{\infty} d\omega\ e^{i\omega t}\ \bar{a}\ (\omega)$$

To compute the velocity from acceleration data

$$V_{(t)} = \int_{\infty}^{t} dt\ a(t)$$

where

$V_{(t)}$ = velocity

$$V_{(t)} = \int_{\omega}^{\infty} dt' \; H(t - t') \; a(t')$$

where

$$H(t - t') = \begin{matrix} 1 & t' < t \\ 0 & t' > t \end{matrix}$$

$$E\{V(t) \; v(t')\} = \int d\omega \; e^{i\omega(t-t')} \left|\bar{h}(\omega)\right|^2 \rho_a(\omega)$$

where

$$\bar{h}(\omega) = \int_{-\infty}^{t} dt \; e^{-i\omega t} \; H(t)$$

$$= \lim_{u \to 0} \int_{-\infty}^{t} e^{-i\omega t + ut} \, dt$$

$$= \lim_{u \to 0} \left[\frac{1}{-i\omega + u} \left(e^{-i\omega t + ut} \right) \Big|_{-\infty}^{\infty} \right] .$$

$$= \lim_{u \to 0} \frac{e^{-i\omega t + ut}}{-i\omega + u} = \frac{i}{\omega} \; e^{-i\omega t} \left|\bar{h}(\omega)\right|^2 = \frac{1}{\omega^2}$$

$$\overline{[V(t)]^2} = E\{V(t)\,V(t)\} = \phi(0)$$

$$= \int_{-\infty}^{\infty} d\omega\; e^{i\omega(t-t)} \left|\bar{h}(\omega)\right|^2 \rho_a(\omega)$$

$$= \int_{-\infty}^{\infty} d\omega\; \frac{\rho_a \omega}{\omega^2}$$

$$\text{RMS} = \overline{V(t)} = \left[\int_{-\infty}^{\infty} d\omega\; \frac{\rho_a(\omega)}{\omega^2} \right]^{1/2}$$

likewise

$$\overline{[x(t)^2} = E\{|x(t)|^2\} = \phi_x(0) = \int_{\infty}^{\infty} d\omega\; \rho_a \frac{(\omega)}{\omega^4}$$

$$\overline{x(t)} = \left(\int_{-\infty}^{\infty} d\omega\; \frac{\rho(\omega)}{\omega^4} \right)^{1/2}$$

Appendix B

First Mode of Vibration For a Cantilevered Beam

(Ref. 16:456-470)

The following derivation of the first mode shape of a cantilevered beam can be found in the reference cited.

The differential equation for a vibrating beam in the shape of a wedge has the form (see Figure 26)

$$\frac{\partial^2}{\partial x^2}\left(EI\ \frac{\partial^2 y}{\partial x}\right) + p\,A\,\frac{\partial^2 y}{\partial t^2} = 0$$

where

$I_{(x)} = 1/12\left(\frac{2bx}{\ell}\right)^3$ = first moment of inertia

$A_{(x)} = \frac{2bx}{\ell}$ = area of the cross section

l = length of the beam

$2b$ = depth at the fixed end

EI = flecural rigidity of the beam

p = mass/unit area

The boundary conditions are

$$\left(EI\ \frac{d^2y}{dx^2}\right)_{x=0} = 0 \qquad \frac{d}{dx}\left(EI\ \frac{d^2y}{dx^2}\right)_{x=0} = 0$$

$$\left(y\right)_{x=\ell} = 0 \qquad \left(\frac{dy}{dx}\right)_{x=\ell} = 0$$

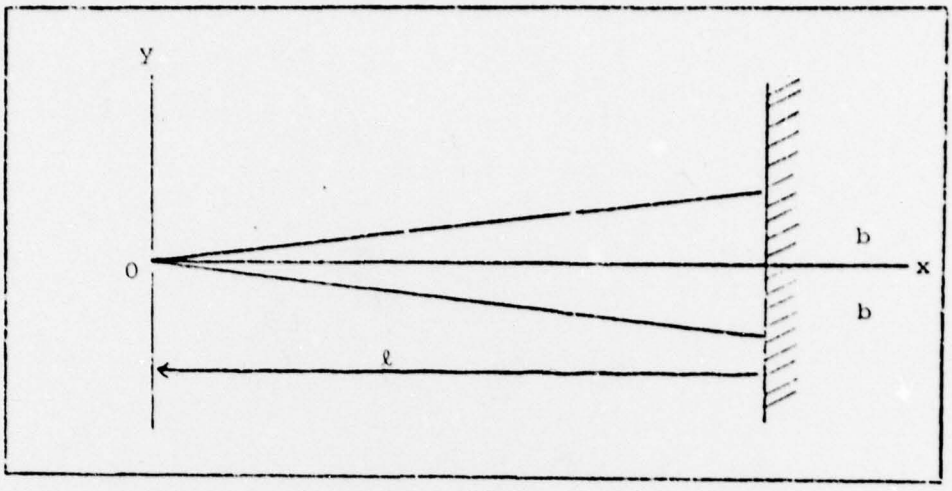

Figure 26. Beam (Ref. 16:466)

The following series satisfies these boundary conditions using the Ritz Method (Ref 16:461).

$$y = a_1 \left(1 - \frac{x}{\ell}\right)^2 + a_2 \frac{x}{\ell} \left(1 - \frac{x}{\ell}\right)^2 + a_3 \frac{x^2}{\ell^2} \left(1 - \frac{x}{\ell}\right)^2 + \ldots$$

As a first approximation

$$y = a_1 \left(1 - \frac{x}{\ell}\right)^2$$

Vita

Kurt F. Schroeder was born on 16 January 1947 in Sparta, Wisconsin. After graduating from high school in Seoul, Korea in 1966, he returned to the United States to attend Lamar University where he received a Bachelor of Science degree in Physics in May 1970. Upon completion of OTS in San Antonio, Texas, he was commissioned in the USAF. He completed flight training and received his wings in 1971. He served as weapon systems operator in the F-4 in the 13 TFS, Udorn, Thailand, and in the 496th TFS, Hahn, Germany until entering the School of Engineering, Air Force Institute of Technology in June 1977.

Permanent Address: 1444 Avenue E
Nederland, Texas 77627

UNCLASSIFIED

SECURITY CLASSIFICATION OF THIS PAGE (When Data Entered)

REPORT DOCUMENTATION PAGE		READ INSTRUCTIONS BEFORE COMPLETING FORM
1. REPORT NUMBER AFIT/GEP/PH/78D-11	2. GOVT ACCESSION NO.	3. RECIPIENT'S CATALOG NUMBER
4. TITLE (and Subtitle) PARAMETRIC ANALYSIS OF STEREOMETRIC TRACKER FOR USE IN TACTICAL AIRCRAFT		5. TYPE OF REPORT & PERIOD COVERED MS Thesis 6. PERFORMING ORG. REPORT NUMBER
7. AUTHOR(s) Kurt F. Schroeder Capt USAF		8. CONTRACT OR GRANT NUMBER(s)
9. PERFORMING ORGANIZATION NAME AND ADDRESS Air Force Institute of Technology (AFIT/EN) Wright-Patterson AFB OH 45433		10. PROGRAM ELEMENT, PROJECT, TASK AREA & WORK UNIT NUMBERS 99912004
11. CONTROLLING OFFICE NAME AND ADDRESS Air Force Avionics Laboratory (AFAL/RWI) Wright-Patterson AFB OH 45433		12. REPORT DATE October 1978 13. NUMBER OF PAGES 104
14. MONITORING AGENCY NAME & ADDRESS(if different from Controlling Office)		15. SECURITY CLASS. (of this report) Unclassified 15a. DECLASSIFICATION/DOWNGRADING SCHEDULE

16. DISTRIBUTION STATEMENT (of this Report)

Approved for public release; distribution unlimited.

17. DISTRIBUTION STATEMENT (of the abstract entered in Block 20, if different from Report)

Approved for public release; IAW AFR 190-17

JOSEPH P. HIPPS, Major, USAF
Director of Information 19 Jan 79

18. SUPPLEMENTARY NOTES

19. KEY WORDS (Continue on reverse side if necessary and identify by block number)

Optical tracking
Image degradation
Correlation
Passive Range Finder

20. ABSTRACT (Continue on reverse side if necessary and identify by block number)

The stereometric range finding technique is used as the basis of an airborne passive tracker. An analysis of the method reveals that angular accuracy is the most critical element in this technique. Range accuracy can be improved by increasing baseline separation. However, the vibration environment of the aircraft becomes worse as the baseline is increased. The results of this investigation indicate that these vibrations counter any gain in resolution. The investigation was hindered by a lack of vibrational data, especially angular vibration data.

DD FORM 1 JAN 73 1473 EDITION OF 1 NOV 65 IS OBSOLETE

UNCLASSIFIED

SECURITY CLASSIFICATION OF THIS PAGE (When Data Entered)